UNIVERSITÉ DU QUÉBEC

MÉMOIRE PRÉSENTÉ À
L'UNIVERSITÉ DU QUÉBEC À CHICOUTIMI COMME
EXIGENCE PARTIELLE
DE LA MAÎTRISE EN INGÉNIERIE

Par

MANDANA JAVAN-MASHMOOL

Theoretical and Experimental Investigations for Measuring Interfacial Bonding Strength between Ice and Substrate

NOVEMBRE 2005

Bibliothèque Paul-Émile-Boulet

UQAC Université du Québec à Chicoutimi

Mise en garde/Advice

Afin de rendre accessible au plus grand nombre le résultat des travaux de recherche menés par ses étudiants gradués et dans l'esprit des règles qui régissent le dépôt et la diffusion des mémoires et thèses produits dans cette Institution, **l'Université du Québec à Chicoutimi (UQAC)** est fière de rendre accessible une version complète et gratuite de cette œuvre.

Motivated by a desire to make the results of its graduate students' research accessible to all, and in accordance with the rules governing the acceptation and diffusion of dissertations and theses in this Institution, the **Université du Québec à Chicoutimi (UQAC)** is proud to make a complete version of this work available at no cost to the reader.

L'auteur conserve néanmoins la propriété du droit d'auteur qui protège ce mémoire ou cette thèse. Ni le mémoire ou la thèse ni des extraits substantiels de ceux-ci ne peuvent être imprimés ou autrement reproduits sans son autorisation.

The author retains ownership of the copyright of this dissertation or thesis. Neither the dissertation or thesis, nor substantial extracts from it, may be printed or otherwise reproduced without the author's permission.

Dedication

I dedicate this thesis in loving memory of my parents who have always been very supportive, understanding and encouraging through my study.

Abstract

This Master study deals with the development of a mechanical technique for measuring interfacial bonding strength of atmospheric ice, using embedded piezoelectric film (PVDF) sensors at the ice/substrate interface. The substrate is an aluminum beam on which PVDF piezoelectric sensors are bonded. The composite beam, formed by an aluminum beam and a deposited ice layer, is submitted to sinusoidal stress at the interface by an electromagnetic shaker on which one end of the beam is clamped. The ice layer is deposited artificially on the aluminium beam from sprayed supercooled water droplets in order to simulate atmospheric icing on structures.

The piezoelectric charge coefficient is used to predict the electric charge density induced on the piezoelectric (PVDF) film which enables us to develop a macroscopic and direct measurement technique for determining mechanical stresses at the atmospheric-ice/substrate interface. All tests have been performed for a frequency close to the natural resonance frequency of the aluminum beam. The tests were carried out on two series of aluminum beams with two different finishes and on Plexiglas.

It may be observed that, in all test series, with an increase in displacement amplitude of the clamped end, the interface stress increases approximately linear until delamination or

ice de-bonding occurrence at the film position. At this specific moment a drastic change in the interface stress occurred resulting from a local redistribution of the bending and shear stress. Hence, the interface stress obtained at this specific moment corresponds to the stress required to de-bond the ice from its substrate (ice adhesion strength). The obtained empirical results demonstrate that ice adhesion strength depends on the surface finish, as it is more finished the adhesion strength is less. The experimental results prove that ice adhesion strength significantly depends on substrate type as the adhesion strength on Plexiglas surface was 100 times less than on the aluminum surface. Within the limitations of the experimental conditions, it was possible using this approach to estimate ice adhesion strengths in accordance with those obtained in literature. This demonstrates the feasibility of this simple ice adhesion testing method.

Résumé

Cette étude porte sur le développement d'une technique mécanique pour mesurer la force d'adhérence de la glace atmosphérique à l'aide d'un film polymère piézoélectrique (PVDF) inséré à l'interface glace/substrat. Dans le cas présent, le substrat est une poutre d'aluminium sur laquelle l'élément piézoélectrique PVDF est collé et sur laquelle la glace atmosphérique est déposée artificiellement à partir de gouttelettes d'eau surfondues. La poutre composite ainsi formée, qui est encastrée à une extrémité au niveau de l'aluminium et libre de l'autre, est soumise à une flexion simple par une excitation mécanique sinusoïdale appliquée sur l'extrémité encastrée dans le plan vertical en utilisant un pot vibrant.

Le coefficient piézoélectrique de charge est utilisé afin de mesurer la charge électrique induite par le film PVDF qui est directement proportionnelle à la contrainte mécanique générée à l'interface glace/poutre, résultante de la contribution de la contrainte en flexion et de cisaillement. Ce principe permet ainsi de développer une méthode de mesure macroscopique et directe afin de déterminer des contraintes mécaniques à l'interface de glace atmosphérique/substrat. Tous les essais ont été réalisés à une fréquence proche de la fréquence de résonance de la poutre composite.

Après avoir étalonné la méthode par une modélisation numérique et dynamique de la poutre en aluminium seule, trois séries d'essais ont été effectuées dont deux avec des poutres en aluminium de rugosités différentes et la troisième avec une poutre identique géométriquement mais constituée de plexiglas. Les résultats obtenus avec des dépôts de glace de quatre millimètres d'épaisseur montrent que la contrainte d'interface augmente linéairement avec l'augmentation de l'amplitude de la contrainte d'excitation jusqu'au décollement de la glace, résultant d'un délaminage progressif initié à l'encastrement et qui se propage vers le milieu de la poutre composite. L'instant où le délaminage atteint le film PVDF est facilement détectable par la lecture du signal délivré par ce dernier qui permet ainsi de déterminer la contrainte mécanique nécessaire pour détacher la glace du substrat. Les résultats obtenus à partir des trois séries montrent que la méthode proposée est valide puisque les valeurs des forces d'adhérence obtenues dépendent de la rugosité du substrat dont l'augmentation entraîne une augmentation de la force d'adhérence et les force d'adhésion dépendent aussi du matériau constituant le substrat avec une force d'adhésion sur l'aluminium environ cent fois plus grande que pour le plexiglas. De plus, les résultats obtenus sont en accord avec les ordres de grandeurs des forces d'adhérence de la littérature.

Ainsi, une méthode simple et originale, basée sur l'utilisation de films polymères piézoélectriques PVDF et permettant des mesures directes de la force d'adhérence de la glace a été développée et validée. Cette méthode a permis de tester différents matériaux pour des épaisseurs de glace de 4 mm. Cependant, l'épaisseur du dépôt de glace n'est pas

une limitation mais l'influence de cette dernière sur la force d'adhérence reste encore à être démontrée.

Acknowledgements

This Masters' research was carried out within the framework of the Industrial Chair on Atmospheric Icing of Power Network Equipment (CIGELE) and the Canada Research Chair on Engineering of Power Network Atmospheric Icing (INGIVRE) at University of Quebec in Chicoutimi (UQAC).

I would like to thank hearty **Prof. M. FARZANEH**, my director for his support, supervision, guidance, encouragement, motivation and patience in this endeavor. I will forever be indebted to you for showing your interest, generous help during my Masters' studies, and providing me the opportunity to work in 'Pavillon de Recherche sur le Givrage', the grandest research laboratory on the atmospheric icing in the world. Special thanks to **Dr. C. VOLAT**, my co-director and mentor for his patience and guidance. I am particularly grateful for all of your time and help during last two years. I would like to thank **Prof. Y. TEISSEYRE** from 'École Supérieure d'Ingénieurs d'Annecy' for showing his interest, time and help during the experiments. I would like to show my deepest appreciations to all of my friends and collaborators who provided assistance in CIGELE Laboratory and other labs of the University of Quebec at Chicoutimi (UQAC). Special thanks to technicians, for all their collaborations. I would like to thank **my family,** especially **my parents** for all of their love and support through the years, you have

always encouraged me to challenge myself, and I enjoy sharing my accomplishments with you.

Finally, I would like to thank **Jalil Farzaneh-Dehkordi** my spouse. Thank you for your true love and endurance support. I look forward to my future with you and to more great moments.

Table of Contents

List of Figures

List of Tables

List of Symbols

Latin Symbols

A	Cross section area
a	Acceleration of the Clamped end
b	Film Width
C	Capacitance of PVDF film
CIGELE	The Industrial Chair on Atmospheric Icing of Power Network Equipment
D	Charge density developed on PVDF film
d	Sinusoidal displacement
d_0	Amplitude of Sinusoidal displacement
d_{31}	Piezoelectric coefficient in charge mode
DAS	Data acquisition system
e	Film length
E	Young's modulus
E_i	Young's modulus of ice
E_s	Young's modulus of substrate
F	Force
$f(x,t)$	External lateral force per unit area

G	Shear modulus
g_{31}	Piezoelectric coefficient in voltage mode
h_s	Substrate Thickness
h_i	Ice thickness
I	Second moment of area of beam cross section about the neutral axis
INGIVRE	Canada Research Chair on Engineering of Power Network Atmospheric Icing
K	The adjusting coefficient in DAS
$k_{amp.}$	The amplification coefficient (amplifier gain)
L	Beam Length; in Appendix: the current gage length
L_0	The initial gage length
L_f	The final gage length
ΔL	The increment of elongation or contraction
M_g	Global bending moment
M_B	Bending moment
N.A.	Neutral axis
P	Load
p	Permittivity
Q	Charge on PVDF film
Q^*	First moment of area about neutral axis
t	Film Thickness

T	Stress induced on PVDF film
V	Shear force
V_{out}	The output voltage of Piezo film
V'	The output voltage of amplifier
$W(x)$	Bending displacement (The solution of spatial equation)
$w(x,t)$	Bending displacement along z axis
z_B	Bottom position of composite beam along z axis
z_i	Neutral axis position along z axis with respect to ice/substrate interface
z_T	Top position of composite beam along z axis

Greek Symbols

β	Flexural wave number
ε	Electrical Permittivity
ε_i	Normal strain ($i = x, y, z$)
ε_L	Longitudinal strain
ε_T	Transverse strain
$\{\varepsilon\}$	Strain matrix
γ	Pulsation of the temporal solution

γ_{ij}	Shear strain ($i, j = x, y, z$)
ν	Poisson's ratio
ν_i	Poisson's ratio of ice
ν_s	Poisson's ratio of substrate
(u, v)	Displacement vector
σ	Normal stress (in Appendix)
σ_x	Bending stress in x direction
$\{\sigma\}$	Stress matrix
ρ	Mass density
θ	The solution of temporal equation
τ	Shear stress
ω	Pulsation of electromagnetic shaker

CHAPTER 1
INTRODUCTION

Chapter 1
Introduction

1.1 General

In cold climate regions, power lines and communication towers are subjected to damage following freezing rain storms. The January 1998 icing event in Quebec, Ontario and the Maritimes clearly illustrates the disastrous socio-economic consequences of damage to power systems, a catastrophe that highlighted the brittleness of electrical networks against such weather events [1]. For high voltage overhead power transmission, the atmospheric ice accretion on wires and structural members combined with wind causes serious failures as mechanical and electrical breakdowns. Indeed, ice accretion on surfaces can affect the operation of critical systems as aircrafts, hydroelectric intakes, communication and power delivery systems, and many other services. Repair costs after a severe storm can be hundreds of millions of dollars for power transmission companies, such as Hydro-One and Hydro-Quebec [1] . In addition electrical outages may depress residents and businesses of heat, water, and power for extended periods. These concerns and problems led relevant Canadian companies and scientific institutions to become aware of the need for developing effective ice accumulation prevention methods. Obviously the need for reliable transmission networks in severe icing conditions highlights the importance

of ice adhesion studies. To the best of our knowledge, few publications are dedicated to icing and de-icing processes and applicable techniques for overhead power lines [2]. That is why the emergence of research in the field of the prevention of ice accumulations seemed necessary and, consequently, the creation of the Canada Research Chair on Engineering of Power Network Atmospheric Icing (INGIVRE)[1], at University of Quebec in Chicoutimi (UQAC) in January 2003. This will generate new opportunities for researchers, in order to achieve better understandings of the problems related to ice accumulation and adherence, and the development of innovative methods to protect electrical networks against atmospheric icing and its impacts.

1.2 Overview of the Problem

While efforts to develop mechanical ice removal techniques have received the most attention, few studies have focused on understanding the basic mechanism of ice adhesion because of its high sensibility to test conditions, e.g., ice type, substrate structure, temperature and test techniques [3]. When water freezes on solid bodies like car windscreens, power cables or aircrafts it is very difficult to remove except by melting. This strong adhesion of ice to other materials is a property of the ice-solid interface. There have been attempts to reduce it but fundamental physics of the adhesion of ice is not yet well understood. Following photo shows frozen utility lines after an ice storm occurred between

[1] NSERC/Hydro-Quebec/UQAC Industrial Chair on Atmospheric Icing of Power Network Equipment (CIGELE) and Canada Research Chair on Engineering of Power Network Atmospheric Icing (INGIVRE), Université du Québec à Chicoutimi, 555 boulevard de l'Université, Chicoutimi, Qc, Canada, G7H 2B1

1900 and 1919. Evidently after one century of technological progress, the problem of ice adhesion on structures has not yet been solved!

Figure 1.1: A Street in Elora after an ice storm - frozen utility lines are pulled over (photographer unknown)

The removal of ice deposits using anti-icing or icephobic materials which would yield zero ice adhesion on an unheated surface has not yet been achieved. A coating cannot prevent ice from adhering to structures. Ice sticks to everything but probably an 'icephobic' coating can reduce the adhesion of ice, and then the ice can be more easily removed (deiced with less force, i.e. wind or natural vibrations). Despite the considerable number of studies no material has been identified as efficient to assure protection against ice accretion. In fact none holds the two main qualities of a true icephobic substance: 1. high effect of reducing ice adhesion, 2. long life-time [4]. The development of new techniques for thawing ice, anti-icing, and the optimization of the existing techniques require an increased knowledge of the physical-mechanical phenomena at the ice/material interface. Make an effort to improve our understanding of properties of the ice/solid interface, the physics and mechanism of the ice adhesion is still a controversial subject. These studies are complementary to any step in the development of effective techniques to prevent ice accumulation. Some efforts have been put into research for commercial icephobic materials; too, little has been regarded to understand icing processes as applied to power lines.

There is no doubt that a greater effort should go in the direction of obtaining a better understanding of icing processes e.g., ice adhesion force instead of waiting for the development of efficient ice repellent materials. The determination of adhesion forces between ice and various surfaces is definitely important for analysis of a number of processes, as it would allow for the selection of more efficient and economical de-icing

techniques. Developing an effective method in order to determine adhesion strength will allow us to quantify necessary mechanical energy at the interface for removal of ice. However, the review of literature shows that few measurement techniques make it possible to macroscopically determine the mechanical stresses at the ice/material interface [5].

The adhesion force is equal to the force needed to separate the ice from the substrate in adhesive failure. Ice adhesion has been measured in a variety of ways but the results are relatively scattered and difficult to compare because adhesion strength is highly sensible to differences in test conditions, e.g., ice type, substrate structure, temperature and test technique.

In the next section, Review of literature, it can be seen that in majority of known techniques, the increasing rate of applied load is instantaneous that means the failure can not be incremental , then cohesive failure[2] is more probable which is undesirable. In some of the methods the load is applied directly on the ice which has a brittle structure. Generally, these methods quantify indirectly the mechanical adhesion forces of ice [3][4][6][7][8][9][10] .Moreover, the majority of the suggested methods are usable only for ice formed by simple freezing, i.e., ordinary ice or oceanic ice. Very few of these methods are applicable to atmospheric ice, which is formed from spraying super-cooled water droplets [9][10]. Consequently, under these conditions, additional studies are necessary in

[2] Cohesive Failure: Failure occurs within ice itself , not at the ice/material interface

order to quantify directly and macroscopically the mechanical stresses that are generated at atmospheric ice/material interface.

1.3 Research Objectives

This research will focus on theoretical and particularly experimental investigations that lead to the development of a macroscopic and direct measurement method for determining interfacial bonding strength at the atmospheric ice/substrate interface using piezoelectric sensors. A method in which the adhesive failure is certain and incremental, which means the failure does not occur within ice and the failure is not instantaneous in all over, respectively. As we all know ice is not strong under vertical and direct load. In other words, in the direct force application on the ice the surface molecules are more susceptible to break than bulk and interface molecules, which means cohesive failure is more probable. One of the advantages of this method is that load is applied indirectly on the ice/material interface.

Developing a macroscopic and direct method has many advantages in order to measure ice adhesion force in different situations, and for many applications. This is made possible by using integrated piezoelectric sensors, which have been utilized more and more in composite materials, in order to sense mechanical stress at the atmospheric ice/substrate interface during experimental tests. Moreover, it is related to the multi-layer materials

technology and properties of their interfaces with regard to a substrate on which a layer of atmospheric ice has been deposited. The preliminary results show that adhesive failure is obtained for a frequency close to the natural resonance frequency of the aluminum beam. Within the limitations of the experimental conditions, it is possible using this approach to obtain ice adhesion strengths in accordance with those in literature. This demonstrates the feasibility of this simple ice adhesion testing method. The challenging objectives of this research can be divided into six stages, as follows:

- A comprehensive review of literature of ice adhesion measurement techniques

- The design of a new and innovative experimental set-up

- The development of a mathematical and analytical model in order to calibrate and to explain the mechanical behavior at ice/solid interface in this particular set-up

- The construction of the experimental assembly and installation

  Obviously, the accuracy of the results depends on the conditions under which the experiments are carried out. This stage relates primarily to establish experimental requirements and the choice of proper configuration, based on the analytical calculations, which must respect certain constraints enumerated previously, e.g., to increase the degree of reproducibility of the experiments. It is also related to

piezoelectric sensors integrated into the acquisition system that measure ice adhesion strength. The specific experimental set-up is described in detail in chapter 4. This set-up allows us to measure contribution of both shear and bending stresses everywhere along the prototype.

- The calibration of the laboratory set-up

This stage primarily consists in calibrating the measurements of mechanical stress at the aluminum surface, without ice accretion, using the piezoelectric elements, which could be done by comparing between the experimental results and the results of analytical modeling.

- The validation of ice adhesion measurements

After calibration, measurements of atmospheric-ice adhesion were carried out and results are compared with the results of literature. This was done for various types of substrates (metallic and Plexiglas) and depending on substrate, different rates of load are applied. The proposed technique is relatively simple and does not require the use of sophisticated equipment, yet allowing measurement of interfacial bonding strength of atmospheric ice.

CHAPTER 2
REVIEW OF LITERATURE

Chapter 2
Review of Literature

2.1 Introduction

Some of the earliest studies of the properties of ice concerned the adhesion of ice to itself which is not in the scope of this work. Experiments to measure the adhesion of ice to other materials can be of various kinds. Few mechanical methods make it possible to measure the mechanical adhesion force of ice on different materials [5]. In the range of ordinary forces, ice is a brittle material and its cohesion force is weaker than its adhesion force, therefore the cohesive failure[3] is more likely than adhesive failure[4]. Thus, the known methods in the field of adhesion measurement are difficult to apply for ice. A simple tensile test with the stress normal to the interface frequently results in fracture within the ice, known as 'cohesive break'. An 'adhesive break' at the interface itself is often observed when a shear stress is applied in the plane of the interface and this geometry is therefore more commonly used for studying the adhesion of ice [5]. It has been found that the adhesive strength depends on the rate of the loading, the surface finish, and the type of material.

[3] Cohesive failure: failure characterized by rupture within the adhesive, e.g. ice
[4] Adhesive failure: failure of the bond between the adhesive and substrate surface

2.2 Adhesion Theory and Mechanism

2.2.1 Mechanism of Adhesion

The mechanisms of adhesion on substrate are not unique. They depend on the substrate and adhesive material, e.g., ice, and the interactions between them. Several theories of adhesion have been presented [11], they are divided into five categories:

1 **Electrostatic**, when two materials are placed in contact, negatively charged electrons are transferred from the surface of one material to the surface of the other material. Therefore materials in intimate contact can adhere due to a transfer of electrical charge between them. Which material loses electrons and which gains electrons will depend on the nature of the two materials. The material that loses electrons becomes positively charged, while the material that gains electrons is negatively charged. This is shown in Figure 2.1. Electrostatic attraction theory is based on Coulomb's law and donor-acceptor interactions such as hydrogen bond[5]. The transfer of electrons across the interface results in positive and negative charges that interact together.

[5] The interaction between an electron-deficient hydrogen atom with a centre of relative electron excess, e.g., electronegative atoms such as F, N, or O

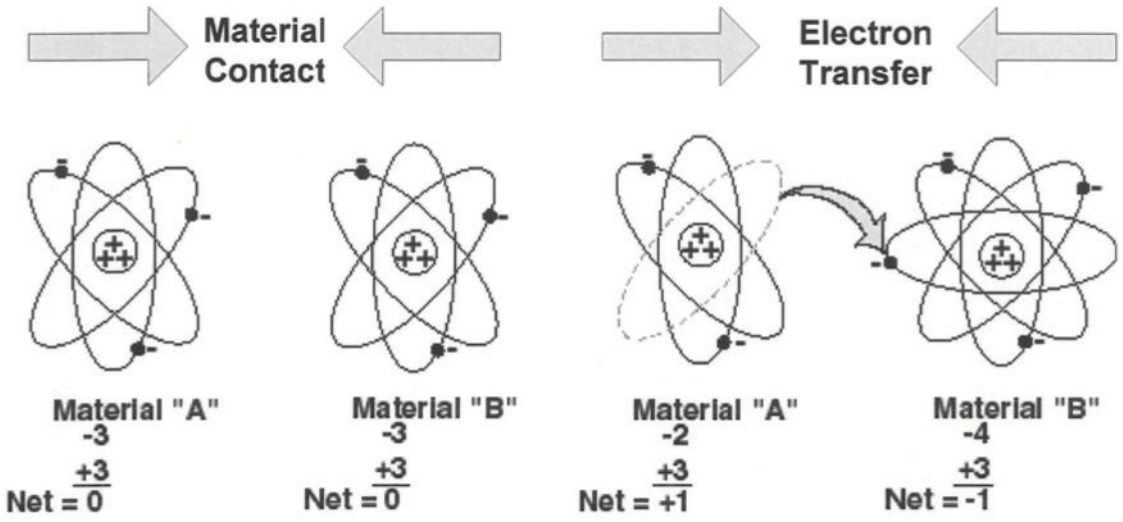

Figure 2.1: Electrostatic attraction due to electron transfer [12]

2 **Diffusion**, Materials adhere because molecules at the surface of one adherent diffuse across the interface into the matrix (lattice) of the other as shown in Figure 2.2, subsequently.

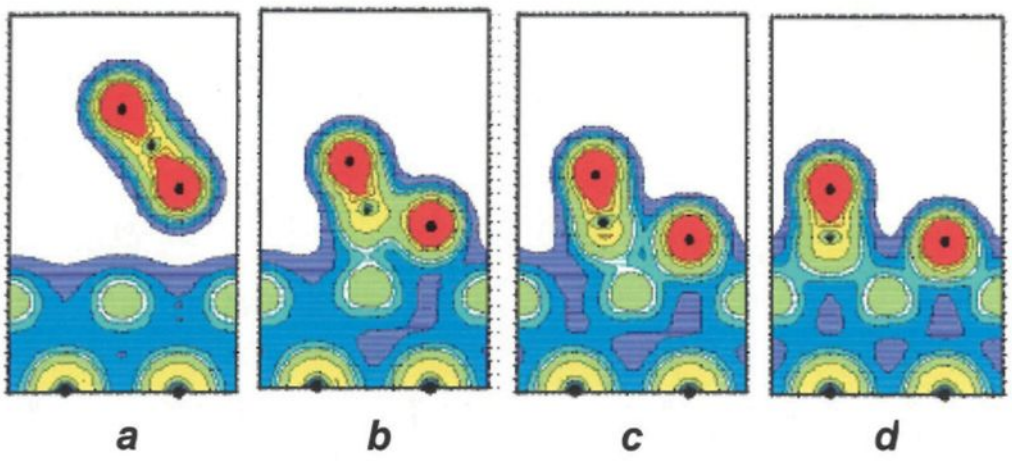

Figure 2.2: The illustration of diffusion on the surface [13]

3 **Chemical**, Materials adhere because chemical bonds are formed between them; in any specific case, a number of different types of bonds can be formed with a single substrate. In Figure 2.3 a chemical bond is schematically illustrated.

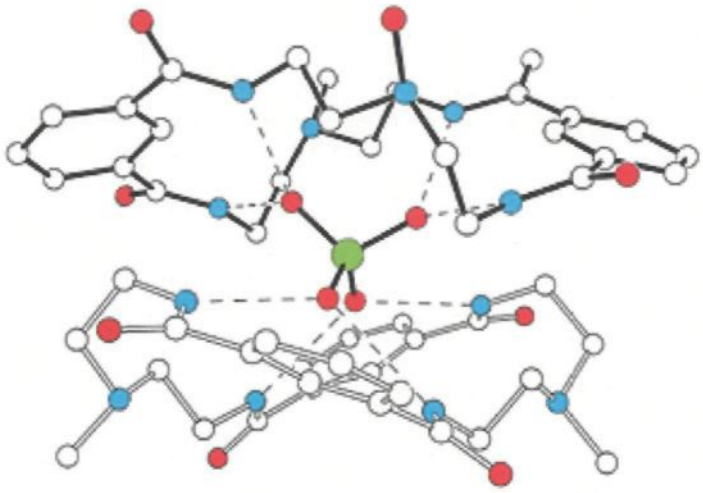

Figure 2.3: Two different materials adhere due to chemical bonds [14]

4 **Mechanical**,

I) Mechanical Interlocking: In macroscopic scale, when the substrate surface contains pores, the interlocking of the solidified adhesive with the roughness and irregularities create a mechanical anchor, seen in Figure 2.4. An adhesive sticks to a substrate because it penetrates into microscopic pores of the substrate and cures thereby forming an interlocking system. In the case of ice adhesion, a water droplet, solidifies and therefore expands and pushes apart the sides of the pore.

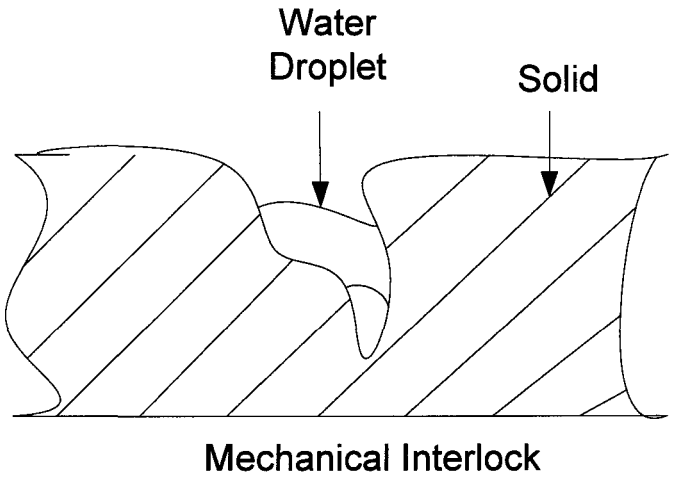

Figure 2.4: Forming of an interlocking system [11]

II) Another type of Mechanical theory of ice adhesion based on a liquid-like transition layer at the ice/air interface and at the ice/substrate interface. The properties of this layer are influenced by the nature of the substrate. The observation of the shear strength at ice/material interface has been interpreted due to sliding on a quasi-liquid layer in the interface [11].

5 **Adsorption** is a process by which a molecule is adsorbed by a substrate, schematically shown in Figure 2.5. It is the result of Van der Waals forces, dipole-dipole or donor-acceptor interactions between the molecule and substrate. The forces of Van der Waals operate between each pair of materials, which is quantitatively small. Polar interactions between ice and aluminum oxide are likely.

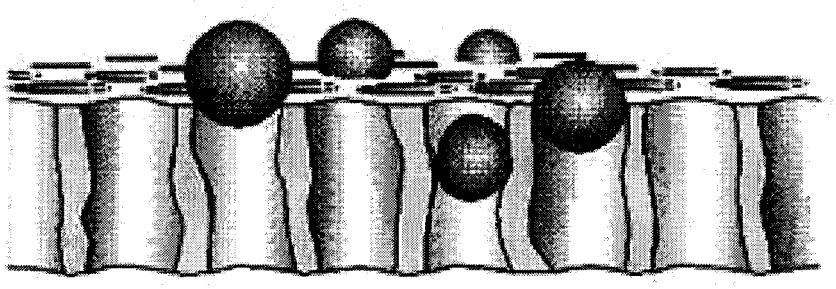

Figure 2.5: Illustration of adsorption of molecules by a substrate [15]

It is found that among these five theories of adhesion, three of them, i.e., adsorption, electrostatic and mechanical interlock interfere in ice adhesion to aluminum [11].

2.2.2 Three Main Adhesion Forces

Intermolecular forces, the attractive forces between molecules, have three types: Dipole-Dipole forces, London dispersion forces (the weakest), Hydrogen bonding (the strongest one). Dipole-Dipole Forces are intermolecular forces that exist between polar molecules. They are active only when the molecules are close together. The strengths of intermolecular attractions increase when polarity increases. The London Dispersion Force is a temporary attractive force that results when the electrons in two adjacent atoms occupy positions that make the atoms form temporary dipoles. Dispersion Forces are present between any two molecules (even polar molecules) when they are almost touching. The London Dispersion Forces are one component of the intermolecular Van der Waals Forces that govern the interactions between two non-covalently bound atoms or molecules [12].

Hydrogen bonding is unusually strong dipole-dipole attractions that occur among molecules in which hydrogen is bonded to a highly electronegative atom.

The force always observed at a surface is the London Dispersion Force and in many instances hydrogen bonds are also found. The generated adhesive force can be very large from a practical viewpoint because of the presence of the hydrogen bonds [16].

2.2.3 Factors that Influence Adhesion Strength

Ice adhesion and its strength are really sensible to test conditions. They are very dependent on temperature, rate of loading, characteristics of the substrate, i.e., its Young modulus and its cohesive strength, type of ice, how the load is applied, surface energy (in microscopic range), and in micro-scales techniques fractures at the interfacial region. For example in the case of its dependence on temperature it is found a linear increase of shear strength with decreasing temperature till -13^0C but the shear stress required for adhesive failure become approximately constant with more falling temperature as shown in Figure 2.6 [18].

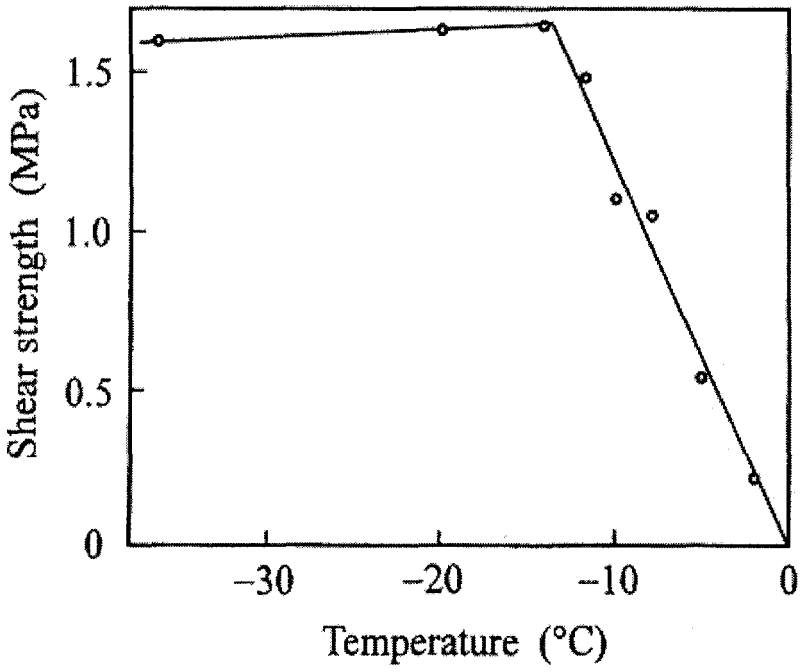

Figure 2.6: Shear strength as a function of Temperature [6]

The problem is further complicated by the fact that deformation and failure depend on the type of the ice and its structure, e.g. ice grain size [12]. Surface energy and adhesion are interrelated. In other words ice on surfaces with low energy has low adhesion.

The other important factor that significantly influences the ice adhesion strength is the rate of load applied in adhesion measurement techniques. Indeed the strength of ice is a function of loads and strain states. Ice exhibits ductile and viscoelastic behavior at low strain rates with no sign of damage or micro-crack formation [5]. At high strain rates, it appears to be brittle, a ductile to brittle transition[6] was observed at intermediate strain rates.

[6] Engineering strain-stress diagram and transition from ductile to brittle is explained in detail in Appendix I.

The structure of ice similar to other materials is not ideal. The rates of loading encountered in practice cover the full range of ductile and brittle behavior. This implies that the viscous or plastic behavior of ice must be taken into consideration for some problems, whereas elastic theory is adequate for others. In its crystalline structure, flaws and cracks are generally observed. In the brittle range, cracks are also created by applying load, and they propagate easily until failure. It is remarkable that cracks and other concentrations play a vital role in the strength and deformation and fracture processes of ice [19]. The fracture is generally initiated by the formation of a crack or the growth of an existing crack, which then spreads through the specimen. The number of cracks and their size increase when a load is applied. However the fracture of ice depends on its grain size, effective surface energy, and elastic constant. Other kinds of defects such as vacancy also exist within the crystal structure. The voids eventually join together to produce large cavities, which lead to the fracture of the structure [16].

As has been indicated, different results may be anticipated using different methods. Hence adhesion force depends on the test techniques which will be applied for ice adhesion measurement.

2.3 Ice adhesion Tests

In the following, a review of various methods to determine ice adhesion strength has been done. This review of different adhesion tests reflects the multifaceted efforts by including new methods.

1. **Lap Shear Tests** [20], where two blocks are pulled apart by tensile stress parallel to the adhesive plane as shown in Figure 2.7. This sandwich configuration makes stress application symmetrical to a central block with two side blocks and two adhesive planes and also some peeling action due to distortion should be avoided. In the second figure with ice as central block it might shatter if pulled but might withstand pushing. Or layers of ice on either side of a central strong block might work. This shear system should require a large total stress for instantaneous overall failure that means the failure can not be incremental.

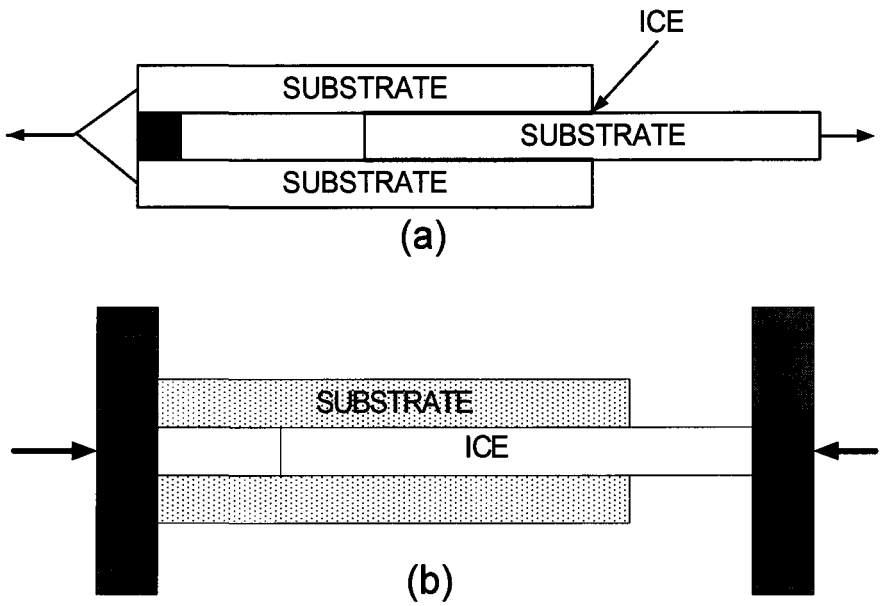

Figure 2.7: Lap shear Tests [21]

2. **Pure Tensile Tests** [20], where two adhered blocks are pulled apart perpendicularly to the adhesive plane. This may result in cohesive failure in substrate, since in most cases a well- made adhered joint is stronger than the substrate. This type of adhesion test with ice on low-adhesion surfaces might be useful. This method entail instantaneous parting over which may result in high gross failure loads compared to some of the methods where failure is incremental.

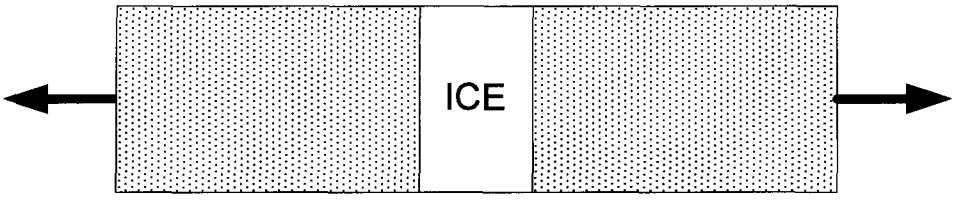

Figure 2.8: Tensile Test [21]

3. **Different types of Torsion Shear Tests** [20], for example in one version the adhesive layer is formed between a fixed plate and a flat disk or annulus, which is then rotated, with measurement of force for failure. In this case intensity of stress or magnitude of strain will vary radially. This may help initiate failure cracks at the periphery, resulting in incremental failure at lower stress which overcomes some of the above problems.

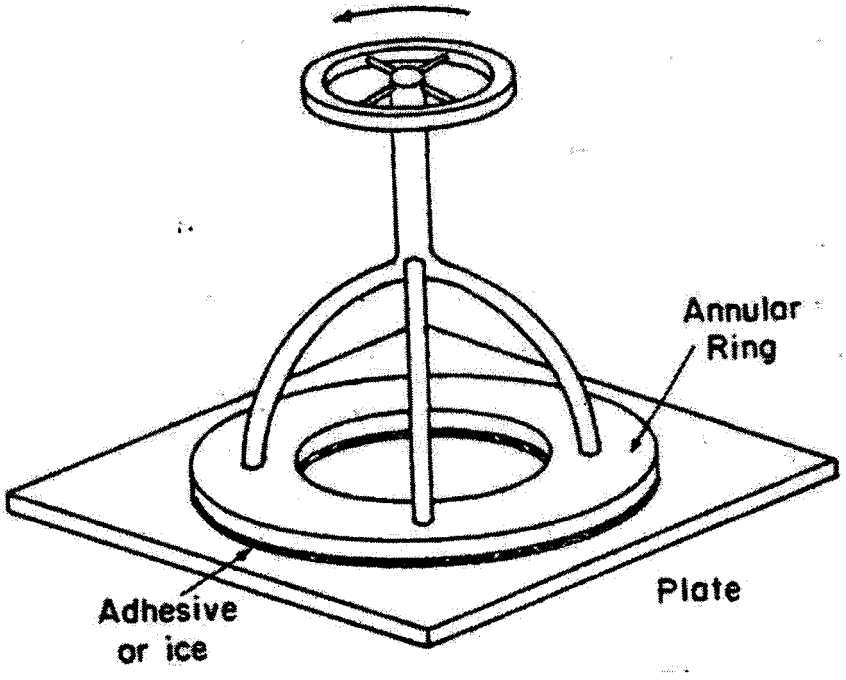

Figure 2.9: Torsion Test [21]

4. **Peel Tests** [20], where the ice is adhered (frozen) to a rigid base and an overlapping free end is pulled away at right angles, measuring the force. This method is adaptable for thin, flexible materials or coatings a specific device could provide for vertical pull. Alternatively, two flexible strips can be adhered and pulled apart. The measured force will be incremental. This method involves mainly tensile stress.

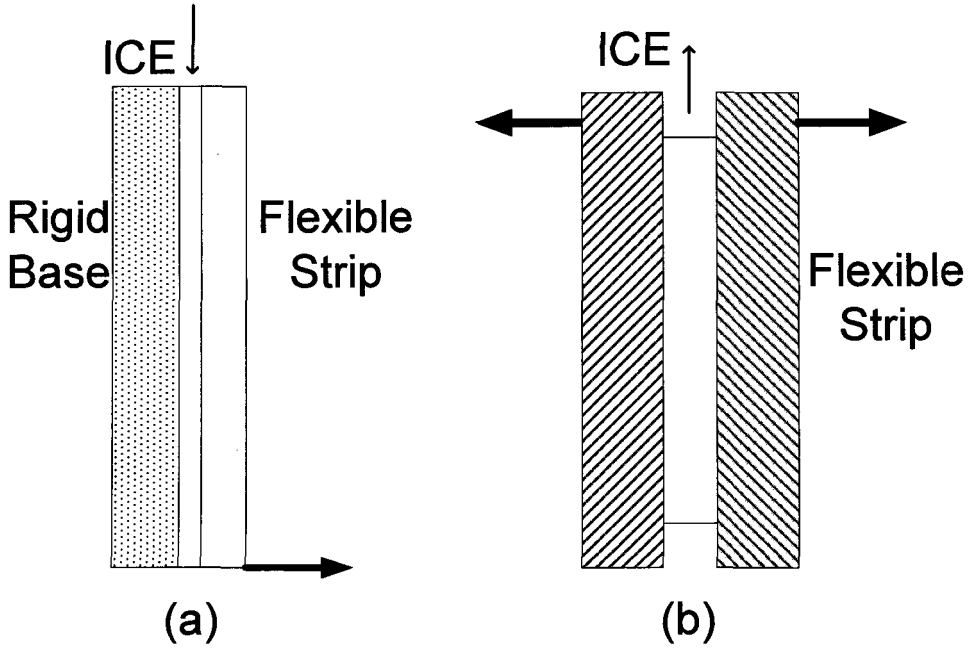

Figure 2.10: Peel Tests [21]

5. **Impact Tests** [16], where the impact is a load which is applied suddenly or with a shock. It always produces a peak stress higher than that produced by a load of the same magnitude if it is applied slowly. The apparatus shown in Figure 2.11 consists of a semi cylindrical bar which is placed with the rounded portion in contact with the ice surface being held firmly in place with U-shaped end pieces. The weight in the tube is raised to a specific height and allowed to drop onto the flat, horizontal upper face of the bar. This is repeated until all the ice is detached. The impact energy is the sum of the energy represented by each impact.

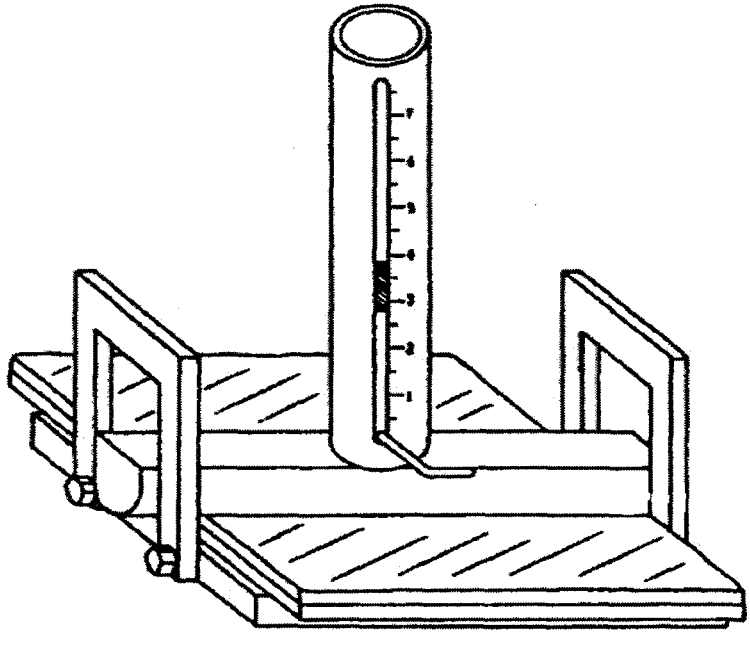

Figure 2.11: Impact Tests [17]

6. **Laser Spallation Technique** [10] is an experimental method for measuring the tensile strength of ice coating to structural surfaces. As shown in Figure 2.12, a laser-induced stress pulse travels through the substrate disc that has a layer of ice grown on its front face. The compressive stress pulse reflects into a tensile wave from the free surface of the ice and pulls the ice/interface apart, given sufficient amplitude. The interface strength was calculated at the interface using a finite-difference elastic wave mechanic simulation. This method shows that the adhesion strength of very thin layers of ice decreases by polishing the substrate surface and by decreasing the temperature. This decrement in the tensile strength can be directly related to the existence of a liquid-like layer that is known to exist on the surface of solid ice till -30° C.

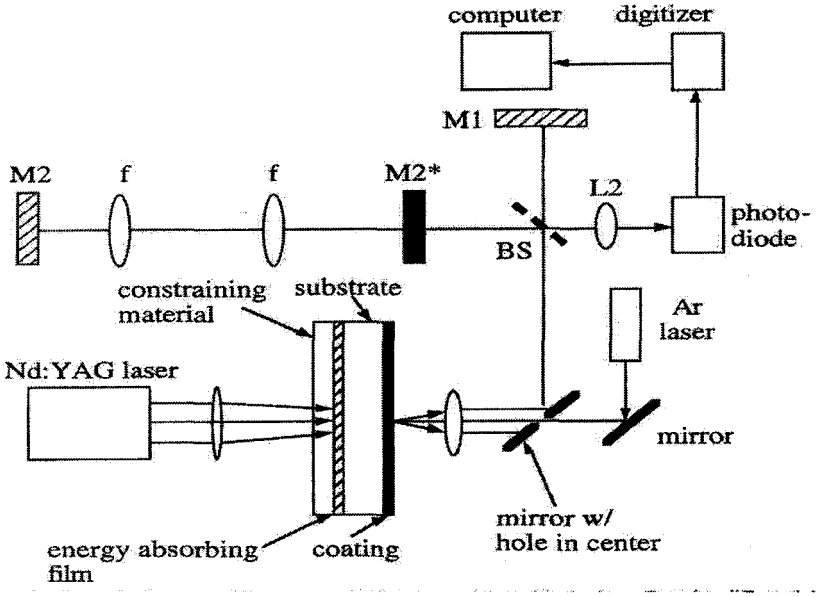

Figure 2.12: Laser Spallation Technique [10]

7. **Atomic Force Microscopy Technique** [21]: this new method using a Nanoscope Atomic Force (AFM) Microscope is employed to determine the adhesion force between an individual particle and a solid surface in order to determine the average value for the adhesion. Micro/Nano scale tests using AFM or Nano indentation instruments can be used to estimate the nature and surface energy, too.

8. **Electromagnetic Tensile Tests** [22], where the interaction of an external magnetic field with an electric current in the coating produces a normal force on the coating and therefore provides a means of measuring the adhesion of the film to its substrate, without requiring any mechanical attachment. This technique is not applicable for ice because of heat generation due to pass the test current. It is designed for adhesion measurement of thin film.

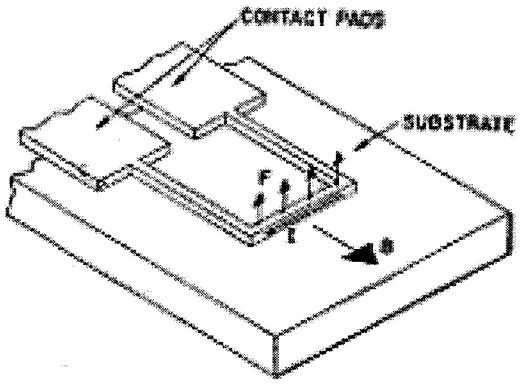

Figure 2.13: Electromagnetic Tensile Test [23]

9. **Blister test** [20], as shown in Figure 2.14, in which air pressure is applied at the center of the adhered interface, the upper (thinner, more flexible) member of which is thereby debond blister-fashion. Forces involved are mainly tensile. In this technique the forces are incremental. Indeed, this method permits a series of measurements on one specimen by interruption of the pressure and noting each debonds location.

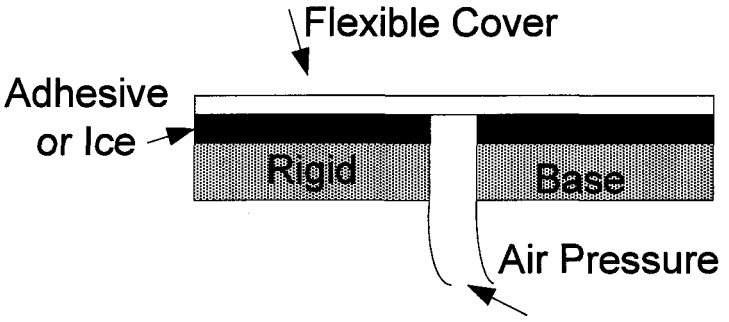

Figure 2.14: Blister Test [21]

10. **Scratch Tests [23]** in which a smoothly rounded diamond tip is drawn across the coating surface and a vertical load, applied to the point, is gradually increased until the coating is completed removed. This method is not usable for ice which has a brittle structure.

11. **Cylinder Torsion Shear Test** [20], where an adhesive layer (ice) is formed between a hollow cylinder and central core, one of which is rotated and the torque measured. Here stress should be uniform and symmetrical at all points. The failure occurs instantaneous in all over.

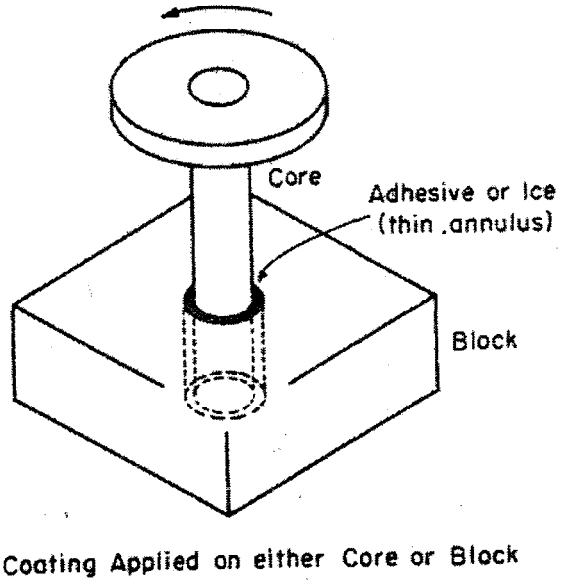

Figure 2.15: Cylinder Torsion Shear Test [20]

12. **Combined Mode Tests** [20], for example combined shear and tensile force might be useful. This could be done by applying a fixed load in one mode while increasing the other till failure. The fixed-variable stress combination should aid in initiation and propagation of cracks to failure.

13. Axial Cylinder Shear Test [20], consists of exerting a force as alternative pull or push to a ring and adhered central core. An axial force may give pure shear. Instantaneous failure all-over is more likely.

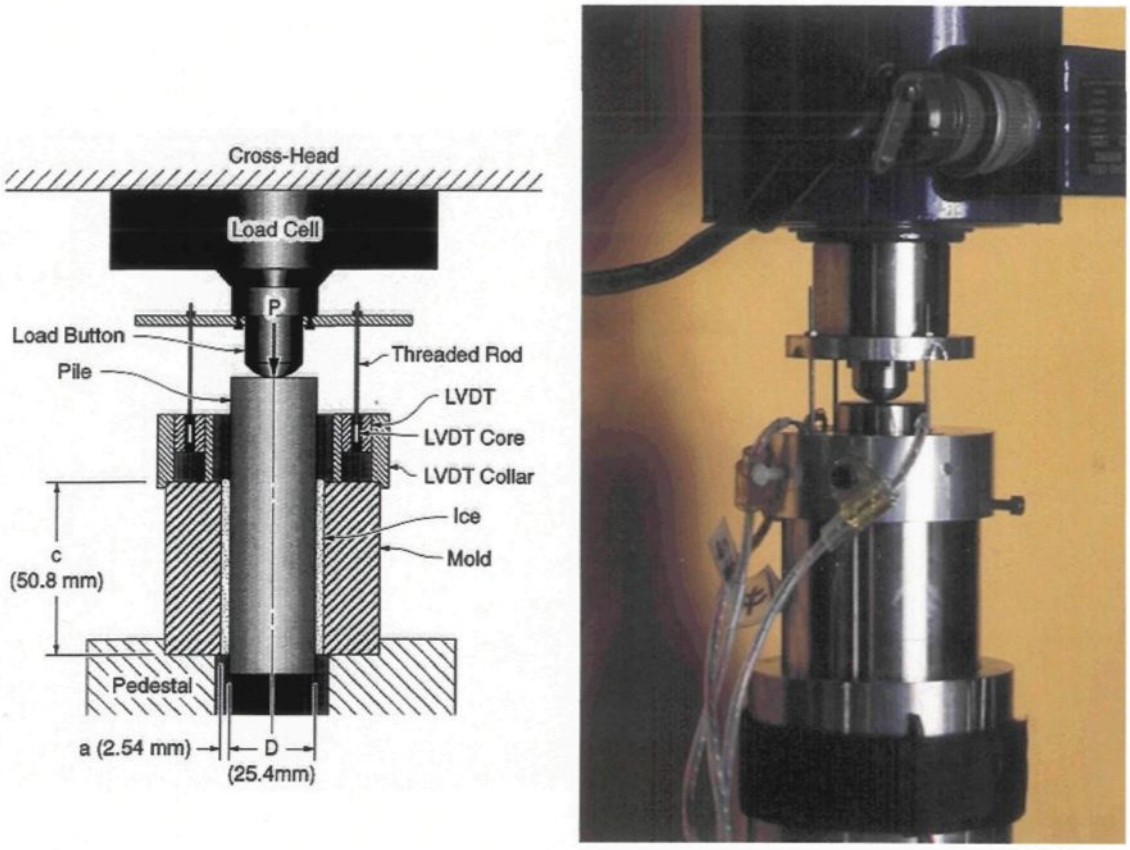

Figure 2.16: Axial Cylinder Shear Test [21]

14. Cone Test [20], for which cone angle $0^0 < \phi < 90^0$. Test H_1 is application of axial force (combination of tensile and shear stress). Test H_2 is application of torsion force (shear stress). In both, instantaneous failure will be occurred. When $\varphi = 90° \equiv$ Lap Shear Test (explained at page 20) While $\varphi = 0° \equiv$

Cylinder Torsion Test (torsion force) and Axial Cylinder Shear Test (axial force).

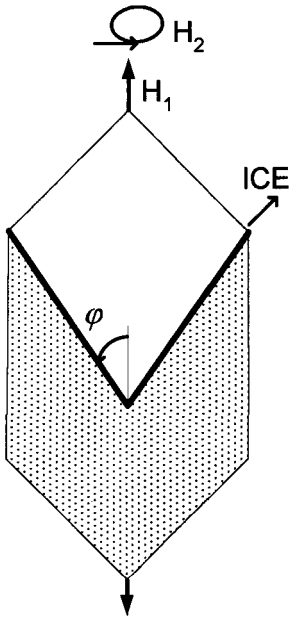

Figure2.17: Cone test [21]

Another simpler method, in theory, uses a beam on which the ice is deposited [4]. A bending moment is applied to the beam by a mechanical impulse which leads to the ice separation. The ice thickness is chosen in order to induce the maximum value of shear stress at the interface which is indirectly deduced from the measurement of the applied force and the displacement of the beam. Since in this method the thickness of the ice coating is selected to the value for which the neutral axis locate at vicinity of the ice/aluminum interface that will be a limiting method. The disadvantages like yielding an indirect value of adhesion force and high sensitivity to the thickness of ice can lead into

some inaccuracies. In addition, this method is not sensitive enough to measure weak adhesion forces, as in the case of ice-phobic materials.

As has been seen the most of these tests are macroscopic and mechanical measurements. In the majority of methods a pulling or pushing force was exercised on the ice to debond it from its substrate. Different results may be anticipated using different methods. For an example, the review of literature [20] shows that in contrast to shear experiments, tensile experiments showed that the adhesive strength under tension is at least 15 times larger than the adhesive strength obtained from shear experiments. This large discrepancy was explained by the assumption of a liquid-like layer between ice and solid interface. In the case of tension, this layer is held together by surface tension forces whereas in shear only fractional forces, which are of much smaller magnitude, have to be overcome [18]. Another note is that the ice solidification is accompanied by expansion. This could affect some of the test schemes, as an example, the temperature of the ice sample must be held constant during the experiment. Also the stress should not be applied during freezing. Because ice is brittle and not strong in either tensile or compressive mode, the stress developed on freezing might cause cracking, producing a cohesive breaking before adhesive failure.

The intention is to measure the force to separate the ice from its substrate in adhesion failure, in other words, the force needed to overcome the adhesion between coating and substrate. In practice however, the cohesive strength of the coating, e.g., ice, and of the

substrate both have an effect on how easy it is to remove the coating. In the case of ice, cohesion force is lesser than adhesion that means the cohesion failure is more likely. Moreover, among the methods used for ice adhesion tests some can only be used for ordinary ice and excludes atmospheric ice formed by the freezing of the super-cooled water drops in contact with structures.

2.4 Conclusion

In conclusion, the basic of an adhesion test involves a load applied to adhesive/substrate system until failure occurs. Shear mode tests, i.e. "Lap Shear Test" or, "Torsion Shear Test" are more common. In the Torsion Shear Test the adhesive layer is formed between a fixed plate and a flat disk, which is rotated, with measurement of force for failure. In "Cylinder Torsion Shear Test" the ice freezes between a hollow cylinder and central core, one of which is rotated and the torque measured. In "Axial Cylinder Shear Test", for which the ice is deposited between a hollow cylinder and central core, the applied force is axial. There are other techniques like "Tensile Tests" and "Peel Tests" where the ice is frozen onto a rigid base and an overlapping free end is pulled away at right angles, measuring the force. In "Impact Test" a load is applied suddenly on the surface of deposited ice till ice detachment. In "Blister Test" a pressure applied at the center of the adhering interface, the thinner and more flexible member of which is thereby debond in blister-fashion with measuring the adhesion force. Another method uses an instantaneous pressure is applied to the ice deposited beam by a mechanical impulse which leads to ice

separation. Ice thickness is chosen in order to induce the maximum value of shear stress at the interface. The high sensitivity to the thickness of ice and insensitivity to measure weak adhesion forces, as in the case of ice-phobic materials, can lead into some inaccuracies.

Most of known methods have many difficulties and defects that would not yield to desired results, e.g. in some of the enumerated techniques increasing rate of applied load is instantaneous, the load is applied directly on the ice which has a brittle structure, the adhesion force is quantified indirectly, the technique is not applicable for atmospheric ice and occurring the adhesive failure is not obvious.

CHAPTER 3
PIEZOELECTRIC SENSORS

Chapter 3
Piezoelectric sensors

3.1 Introduction

Piezoelectricity, Greek word for "pressure" electricity was discovered by the Curies brothers more than 100 years ago [24]. They found that quartz changed its dimensions when subjected to an electrical field, and conversely generated electrical charge when mechanically deformed. By the 1960's researchers had discovered a weak piezoelectric effect in whale bone and tendon. This began an intense search for other organic materials that might exhibit piezoelectricity. In 1969, Kawai [25] found very high Piezo-activity in the polarized Fluoropolymer, Polyvinylindene Fluoride (PVDF). While other materials like PVC exhibit the effect, none are as highly piezoelectric as PVDF. Today piezoelectric polymer sensors are among the fastest growing of the technologies within the sensor market and there have been an extraordinary number of applications [24].

The most important uses of active/smart material, e.g., piezoelectric, are application as transducer, means sensor and actuator, based on their electromechanical coupling effects, which also constitute a major subject of current research regarding so-called smart materials and structures. Smart structures are being used in a wide range of products. The

Hubble Space Telescope contains smart materials for correcting optical efficiencies, and chip fabrication equipment includes PZT actuators to cancel undesirable vibrations. Smart materials that incorporates 'sensors (nerves), actuators (muscles), and computers (brains)' can be thought of something that takes input energy in one form and converts it to output energy in another form. Depending on the behavior of different smart materials, they may be more suitable for one application or another [26][25] .

Nowadays, Piezoelectric Fluoropolymer Film, or Piezo Film, is an enabling sensor technology with unique capabilities. Piezo Film produces voltage in proportional response to compressive or tensile mechanical stress or strain, making it an ideal dynamic strain gage as shown schematically in Figure 3.1. Successful applications have been developed across a vast dynamic range from sensing nanostrains to measuring explosive-level forces (Mbar). Piezo Film's stress constant (voltage output per stress input) is about 10 times higher than other piezoelectric materials such as ceramics and quartz. It makes a highly reliable vibration sensor, accelerometer and switch element [24].

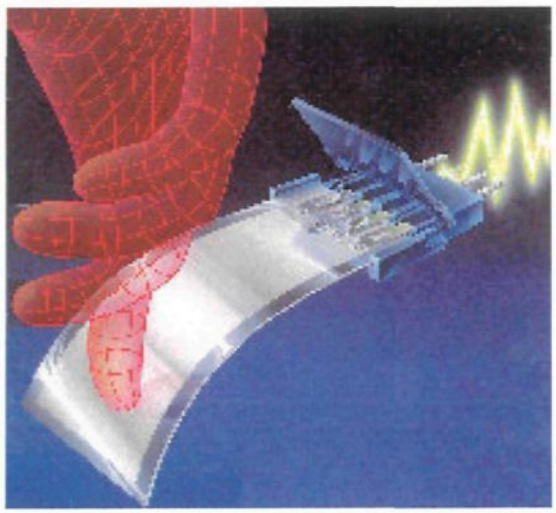

Figure 3.1: Like water from a sponge, piezoelectric materials generate charge when squeezed, making an ideal strain gage [14]

Conversely, Piezo material undergoes a proportional change in dimension under the influence of an applied electric field at frequencies from DC to 100 MHz as schematically seen in Figure 3.2. This property, as well as the film's low impedance, makes Piezo ideally suited for high fidelity transducers operating throughout the high audio (>1KHz) and ultrasonic (up to 100MHz) ranges.

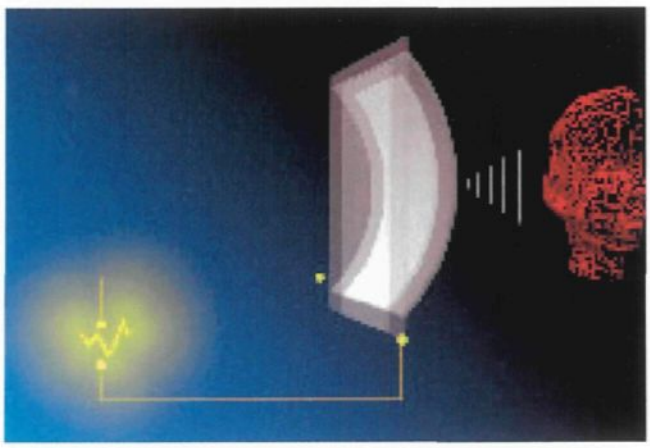

Figure 3.2: Piezo also changes dimension with applied voltage for high fidelity transmission[14]

Piezo Film is robust, thin, with low weight and low mass, so it doesn't attenuate vibrations in the material to which it is attached. Piezo can be formed into cable (available in spools up to 1 mile in length) for applications such as perimeter security. Piezo Film and Piezo Cable can withstand storage and operating temperatures from -40° C to 85° C.

3.2 Piezoelectric Films Properties

Piezoelectric films are light, flexible, and available in wide variety of thicknesses and large areas. They have high sensitivity to mechanical load and small variation in it, flat response over a wide frequency area, and they have also wide frequency range of application from 0.001 Hz to 10^9 Hz [24]. Their output voltage is 10 times higher than Piezo ceramics for the same force input. Due to their low mechanical impedance a number of piezoelectric films can be placed along structure without drastically affecting its mechanical properties. Other characteristics are high mechanical strength and impact resistant, stability confronting chemical components. They are especially interesting due to their high sensitivities to small variations in applied loads. They can be easily manufactured into desired shapes and unusual designs, miniaturized, mounted on, and integrated into the main structures and can be also glued with the commercial adhesive as we have done in our set-up. When extruded into thin film piezoelectric polymers can be directly attached to a structure without disturbing its mechanical motion. Piezo film is well suited to strain sensing application requiring high sensitivity. As mentioned before, operating properties of Piezoelectric materials can be divided into two branches depending of application as

actuator or sensor: Electrical to Mechanical Conversion; i.e., actuator applications and Mechanical to Electrical Conversion; i.e., sensor applications.

In actuator applications many researchers have shown that the vibration control of a structure can be realized by applying an adjustable electric field to a piezoelectric integrated with the structure. As a simple example of this method is sensing and suppressing vibrations of special tables on which very sensible microscopes have been installed. Indeed the application of piezoelectric as an actuator seems an active control of vibration of structures. In fact the active vibration control of flexible structures using piezoelectric materials has been a great interest to many researchers due to their higher potential for shape control, vibration suppression, noise attenuation and damage detection in the past decades as it may be one of the major aircraft designs aspects, which is out of the scope of this study.

In application as a sensor studying the Mechanical to Electrical Conversion is more interesting. Indeed, the sensitivity of Piezo film as a receiver of mechanical work input is awesome. In its simplest mode the film behaves like a dynamic strain gauge except that it requires no external power source and generates signals greater than those from strain gauge after amplification. This extreme sensitivity is largely due to its format. The low thickness of the film makes in turn a very small cross-sectional area, thus relatively small longitudinal forces create very large stresses within the material. This aspect enhances the sensitivity parallel to mechanical axis of the piezoelectric film, which is defined in section

3.4. Some sensor applications of Piezo film are enumerated as in musical instruments, traffic sensors, accelerometers, medical probes, speakers, microphones, impact sensors; i.e., impact printers and sport scoring, switches; i.e., switches for automated process, panel switches, door closure switches, beam switches, and snap-action switches.

If the smart materials are to be used as sensors, they must be integral with the structural material whose strain is of interest such as this project. For an example of an application as a sensor, one applies polyvinylindene fluoride (PVDF) for designing very large, extremely low weight optical sensing systems in space. The primary component of the system is an unsupported laminated reflector consisting of two layers of piezoelectric film, such as PVDF in a bimorph configuration and a single layer of shape memory alloy (SMA), such as Nitinol. The structure will be coated with a reflective surface on one side to function as the primary reflector of a large telescope. The shape of the structure will be controlled in space by scanning an electron beam across the piezoelectric surface, causing local deformations at places where electron charges are deposited. Upon deployment in space, the Sun's heat will activate the Nitinol causing the membrane to deploy to its final configuration with minimal surface wrinkles. An electron beam will be made responsive to an optical figure sensor, observing the shape of the structure, and will stimulate the PVDF layers to correct surface wrinkles and control the curvature of the reflector.

As mentioned earlier, Piezo film's function also depends on temperature variations, as shown in Figure 3.3, Note that d_{3n} and g_{3n} are the fundamental piezoelectric coefficients for charge and voltage, respectively, which are explained in detail in section 3.4.

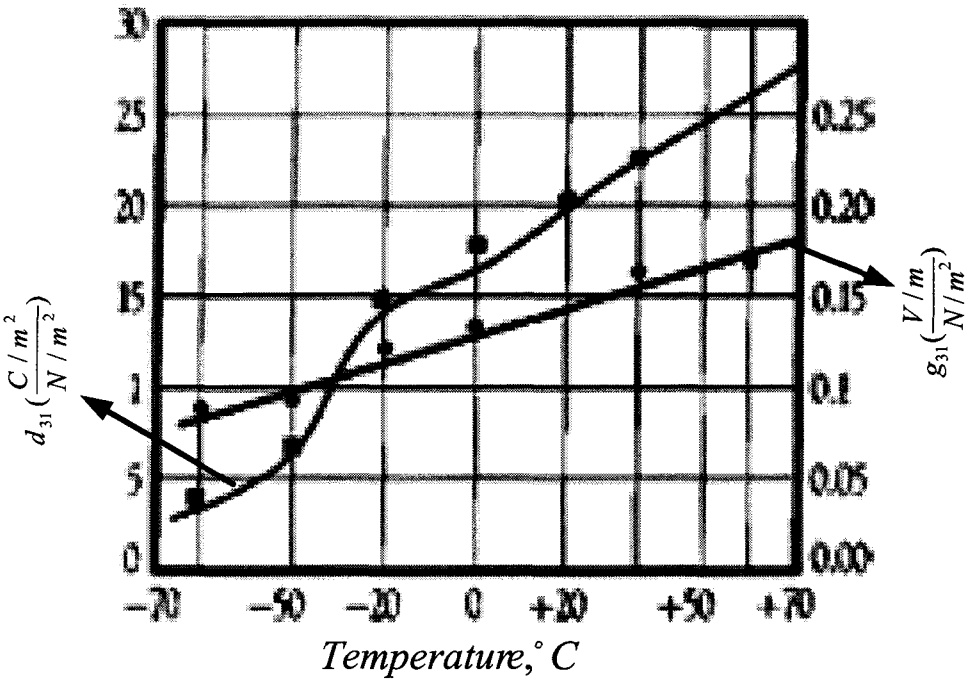

Figure 3.3: Temperature coefficient for d_{31} and g_{31} constants for PVDF film [24]

Many of Properties of Piezo film change with temperature, these properties are reversible and repeatable with temperature cycling [27]. Figure 3.3 shows the reversible temperature effects on d_{31} and g_{31} coefficient for PVDF. Piezo films have been shown to offer excellent transducer properties at very low (cryogenic) temperature. In this study due to the experimental set-up the mechanical stress is applied in the 1-direction shown in Figure 3.6 and piezoelectric films were exposed to -12° C.

Figure 3.6 and piezoelectric films were exposed to -12° C.

3.3 Piezoelectric Film as Source Capacitance

Perhaps the most important characteristic after the piezoelectric property is Piezo film's capacitance. Capacitance is a measure of any component's ability to store electrical charge and is always present when two conductive plates are brought close together. In case of piezoelectric films the conductive plates are the electrode metallized onto each surface of the film[7]. PVDF has a high dielectric constant compared with most polymers, with value about "12" relative to the permittivity of free space. Obviously the capacitance of the element will increase as its plate area is increases. Capacitance also increases as the film thickness decreases. These factors are formally related in the following equation:

$$C_0 = p\frac{A}{t} \qquad \text{Eq.3.1}$$

where C_0 is the capacitance of the film, p is the permittivity, A is the overlap area of the film's electrodes, and t is the film thickness.

Figure 3.4 draws out an electrical equivalent of the Piezo film element. For the equivalent

[7] The capacitance of the capacitor is strongly affected by the properties of the dielectric serving between the electrodes, and the measure of the insulator's capacity to store charge is given by its dielectric constant or permittivity.

circuit, there are two models- one is a voltage source in series with a capacitance, the other a charge generator in parallel with a capacitance.

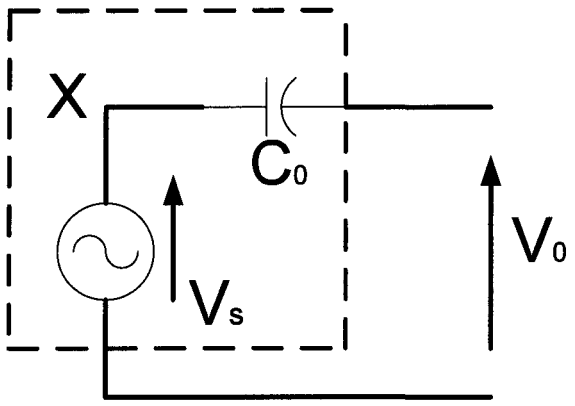

Figure 3.4: Piezoelectric film as a simple voltage generator

Figure 3.4 demonstrates the voltage source which is more common in circuit analysis. The dashed line represents the "contents" of the Piezo film component. The voltage source V_S is the piezoelectric generator itself, and this source is directly proportional to the applied pressure or strain. Our purpose is not to elaborate further calculations. The main point is that this source voltage will absolutely follow the applied pressure, on other words, piezoelectric film is a "perfect" source, a great advantage as a sensor. Note, the film's capacitance, C_0 is always present and connected when the "output" of the film at the electrodes is monitored, the node X can never be accessed, and V_O is open circuit voltage. Note, the voltage source amplitude is equal to the open circuit voltage of Piezo film and varies from micro volts to 100's of volts, depending on the excitation magnitude.

Figure 3.5 shows an equivalent circuit as a charge generator. This equivalent circuit has film capacitance C_f and internal film resistance R_f. The induced charge Q is linearly proportional to the applied force as described earlier. As in this study, in low frequency applications, the internal film resistance is very high and can be ignored. The open circuit output voltage can be found from the film capacitance; i.e. $V = \frac{Q}{C_f}$.

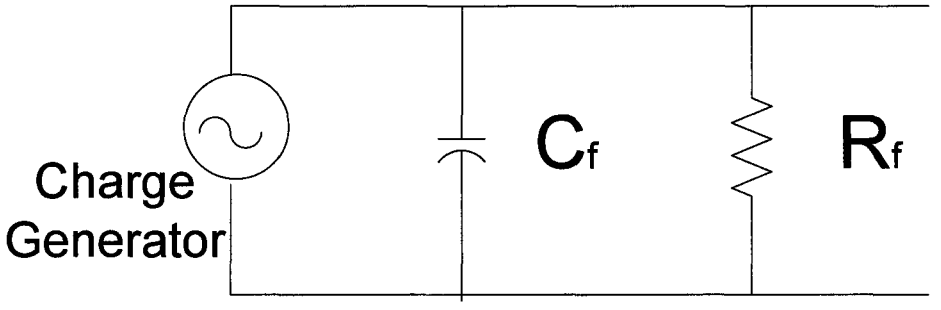

Figure 3.5: Equivalent circuit as a charge generator

3.4 The Fundamental Piezoelectric Equations

The amplitude of the signal generated by the piezoelectric film is directly proportional to mechanical deformation. The resulting deformation causes a change in the surface charge density of the material so that a voltage appears between the electroded surfaces. It seems necessary to introduce the fundamental piezoelectric coefficients for charge and voltage, d_{3n} and g_{3n}, respectively. They predict the charge density (charge per unit area)

and voltage field (voltage per unit thickness) developed by the Piezo film, respectively. Piezoelectric charge and voltage coefficients are each assigned two subscripts: one refers to the electrical axis, the other to the mechanical axis as shown in Figure 3.6. Because Piezo film is thin the electrodes are applied to the top and bottom film surfaces. The electrical axis is always "3" as the charge or voltage is always transferred through the thickness of the film.

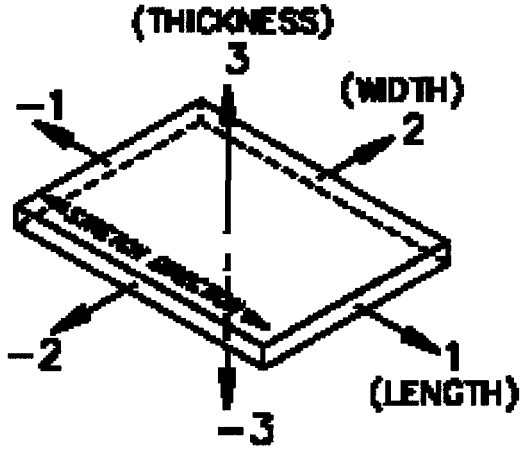

Figure 3.6: Classification of Piezoelectric axes [24]

The mechanical strain can be measured on 1, 2 or 3 since the stress can be applied to any of these axes. It is concluded that piezoelectric materials are anisotropic that its mechanical response differs depending upon the axis of applied mechanical stress. Hence a particular attention seems necessary for taking into account the directionality.

For Mechanical to Electrical Conversion the fundamental piezoelectric equation **in charge mode** is given by [24],

$$D = Q / b.e = d_{3n}.T_n \qquad \text{Eq.3.2}$$

where D (C/m^2) is charge density developed on the film, Q (C) is net charge on the film, $b.e$ (m^2) is Piezo film's electrode area, as shown in Figure 3.7, d_{3n} $(pC/m^2)/(N/m^2)$ is the piezoelectric coefficient in charge mode, and T_n is the mechanical stress applied in the n-direction. In conclusion the charge developed on the piezoelectric film can be expressed as,

$$Q = b.e.d_{3n}.T_n \qquad \text{Eq.3.3}$$

Whereas **in voltage mode** the open circuit output is given by,

$$V = g_{3n}.t.T_n \qquad \text{Eq.3.4}$$

where g_{3n} is appropriate piezoelectric coefficient in voltage mode, and t is the film thickness, as shown in the Figure 3.7.

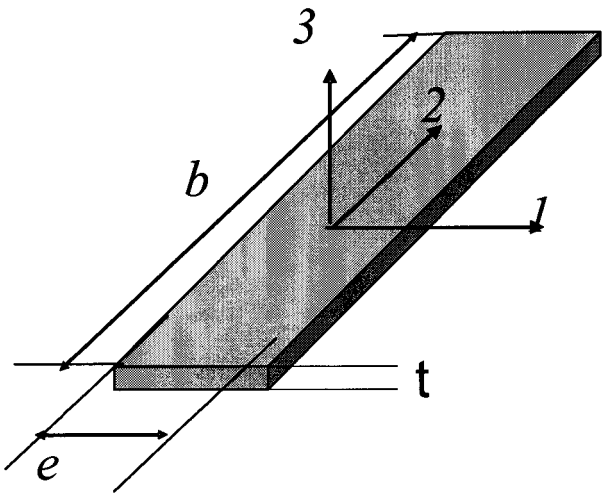

Figure 3.7: Dimensions of film with length of e width of b and thickness of t

Hereafter in this research, for measurement purpose, piezoelectric film is used to assess the adhesion force at the ice/substrate interface. In the following Table almost all typical physical characteristics of PVDF films are shown [24].

Table 3.1: Typical properties of Piezo film [24]

Symbol	Parameter	PVDF	Units
t	Thickness	28	μm (micron)
d_{31}	Piezo Strain constant	23	$10^{-12}\frac{C/m^2}{N/m^2}$
d_{33}		-33	
g_{31}	Piezo Stress constant	216	$10^{-3}\frac{V/m}{N/m^2}$
g_{33}		-330	
C	Capacitance	380	pF/cm^2 @ 1kHz
Y	Young Modulus	2-4	$10^9 N/m^2$
ε	Permittivity	106-113	$10^{-12} F/m$
$\varepsilon/\varepsilon_0$	Relative Permittivity	12-13	_____
ρ_m	Mass Density	1.78	$10^3\ kg/m^3$
	Temperature Range	-40 to 80	$^\circ C$

3.5 Conclusion

As it is mentioned later, piezoelectric film, in sensor application, develops an electrical charge proportional to a change in mechanical stress. In conclusion some of the most

important characteristics of PVDF film for which it has been selected in this study are enumerated below:

1 Small thickness in micron order

2 Lightness

3 Flexibility (it can be easily manufactured into desired shapes, miniaturized, mounted on, and integrated into the main structures)

4 Excellent mechanical strength

5 High sensitivity to mechanical load

6 High sensitivity to small variation in mechanical load

7 Low mechanical impedance (because of this property a number of PVDF films can be placed along the structure without dramatically affecting its mechanical properties.)

8 In this study it can allow a direct measurement of ice adhesion at ice/substrate interface, and

9 It can allow applying any ice thickness, by measuring the contribution of shear and bending stress simultaneously.

CHAPTER 4
THEORY AND CALIBRATION

Chapter 4
Theory and Calibration

4.1 Introduction

In order to describe the stress-strain behavior of ice under loading, physically based models can be used not only as predictive tools, but also as calibration tools for the experimental set-up. The successful development of physically based model is contingent on our understanding of the mechanisms underlying the mechanical properties of ice.

The physical principle of the work is that the ice adhesion strength is equal to the substrate surface stress subjecting to ice at ice/material interface at the time of ice adhesive failure. Different mechanical methods for measuring ice adhesion as well as factors influencing such measurements are briefly reviewed earlier in chapter 2. The purpose of this research is focusing on the development of a mechanical, macroscopic, and direct technique for measuring this strength at ice/material interface. This goal is achieved by using embedded piezoelectric film sensors at the ice/substrate interface. Indeed, a similar technique was previously used successfully for the measurement of interfacial energy and shear stress in composite material [28].

One of the main advantages of this configuration is that the thickness of ice or substrate is not confined by the position of the neutral axis, as in the case of the presented method in [4]. In this configuration, adhesive failure is more likely, because of the creation of the shear stress at interface. The rate of applied load is incremental and the load is applied on the substrate surface not on the ice directly which has a brittle structure. Ice is not strong under the direct load, due to its open chemical structure. If the load is applied directly to the surface of the sample the molecules on the surface are more susceptible to breaking than bulk and interface molecules, therefore cohesive failure is more probable.

The aim of this chapter is to present theoretical investigations and the experimental set-up of this technique and calibration of piezoelectric response. In theoretical approach, the analytical solution of an aluminum beam, driven into harmonic vibration is obtained. Theoretical equations of the bending stress due to a vibrating load in a cantilever beam are derived. A set of presumptions and criteria has been established and used to evaluate a suitable set-up for empirical studies. Prototype configuration has been constructed in CIGELE laboratory. Methodology presented later, has been established particularly for measuring ice adhesion strength. Detailed measurements were carried out and comparisons made between the experimental results and literature.

In order to calibrate our set-up and also enter the proper coefficient in the program of data acquisition system, first a few tests for measuring the stress induced on the beam surface

with the help of PVDF films were performed, of course without ice. Then a comparison was done between:

- The calculated value of theoretical bending stress at the beam surface and,
- The practical tests.

4.2 Analytical Modeling of Beam and its Deflection

4.2.1 Beam Modeling

Figure 4.1 shows the configuration used for modeling. The proposed technique for measuring ice adhesion is based on the bending vibrations of a beam composed of an aluminum substrate and an ice layer deposited on it. As illustrated in Figure 4.1, one end is free to move and the clamped end is fixed onto an electromagnetic shaker in order to produce a desired sinusoidal displacement. Since ice is a brittle material, only the aluminum beam is clamped.

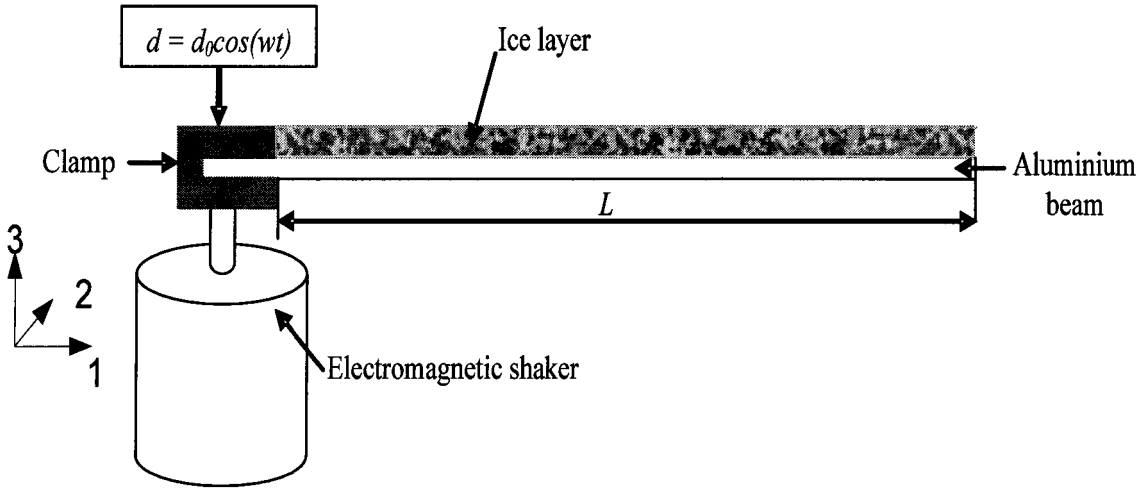

Figure 4.1: A composite beam, composed of an ice layer deposited on an aluminum beam, clamped onto an electromagnetic shaker at one end

The beam is characterized by the following dimensions: h_s thick (3-direction), b wide (2- direction) and L long (1-direction). The ice layer is deposited on this aluminum substrate with the same length and width. Note that the reason for which an aluminum substrate was chosen is that the transmission line conductors generally are made in two parts, a steel core and outer aluminum wires which are exposed to atmospheric icing. The conductor material is made from aluminum or copper. In the North America aluminum is a common material used for conductors.

The clamped end fixed onto the electromagnetic shaker is subjected to a sinusoidal displacement as $d = d_0 \cos(\omega t)$, where d_0 is the maximum normal displacement of the clamped end, and ω is the pulsation of the electromagnetic shaker. Note that there is no direct pressure on the ice. In this particular set-up, the composite beam undergoes small

deflections in its linearly elastic region. As a result of the sinusoidal displacement, the composite beam is subjected to both shear[8] and bending[9] stress. Figure 4.2 represents the bending stress repartition in aluminium and ice considering their Young moduli. Figure 4.3 illustrates both shear and bending stress. Note in reality they are not in the same plane as illustrated in this figure. The shear stress is in yz plane while the bending stress is in xz plane, which illustrated clearly in Appendix, Figure A.2. The Piezoelectric films can be placed on the aluminum surface before ice deposition. The piezoelectric film thickness ($28\,\mu m$) is very thin compared to the substrate and ice thickness. As stress distribution varies along the beam and is a function of 1-direction, x, then the piezoelectric films length is set relatively small in order to sense homogenous stress while their width is the same as the beam. Moreover, due to low mechanical impedance of piezoelectric films, the placement of many of them along the substrate has no influence on the mechanical properties of the structure. Hence, the mechanical influence of the piezoelectric film is not taken into account.

In stress analysis terminology, this problem was considered as a static, linear, temperature-independent problem, isotropic as well as homogeneity of beam. The shear stress is considered to be constant all along the neutral axis. Initial strains may have various causes, including temperature change and swelling due to moisture and radiation, however

---

[8] Shear Stress tends to deform the material without changing its volume, usually by "sliding" forces - torque by transversely-acting forces. The shape change is evaluated by measuring the change of the angle's magnitude (shear strain).

[9] Bending Stress: Force per unit area acting at a point along the length of a member resulting from the bending moment applied at that point.

they are not taken into account. It is assumed that the composite beam width b is small compared to its length L. The stress, T_2 and the deformation in the 2-direction normal to the (*13*) plane seen in Figure 4.3, u_2 are considered to be equal to zero. Similarly, the composite beam thickness $h_i + h_s$ is small compared to its length L . The stress, T_3 and the deformation, u_3, in the 3-direction normal to the (*12*) plane, shown in Figure 4.3, are considered respectively to be equal to zero. However the local deformation, u_3, of the beam is zero in the 3-direction but the beam deflection *W(x)* in this direction is not zero. Note that the beam vibrates in relatively small finite amplitude. Indeed, when a sinusoidal displacement, d, is set in motion at the clamped end of the composite beam, a bending moment, M_B, is induced and lead to the appearance of a stress, T_1, at the ice/aluminium interface. This stress is the result of the contribution of the shear and bending stresses. From Figure 4.3, it can be observed that the resulted stress at the ice/ aluminium interface is directly linked with the position of the neutral axis[10] (N.A.) and, consequently, with the thickness of the ice layer. Along the neutral axis the bending stress is equal to zero whereas the shear stress has its maximum value. This beam transmits a shear force and a bending moment. Note that the x axis must be replaced from the plane of interface and located along the undeformed neutral axis of the beam. Therefore the first step is determining the neutral plane position.

[10] Definition and formulation of neutral axis is explained in section 4.2.2

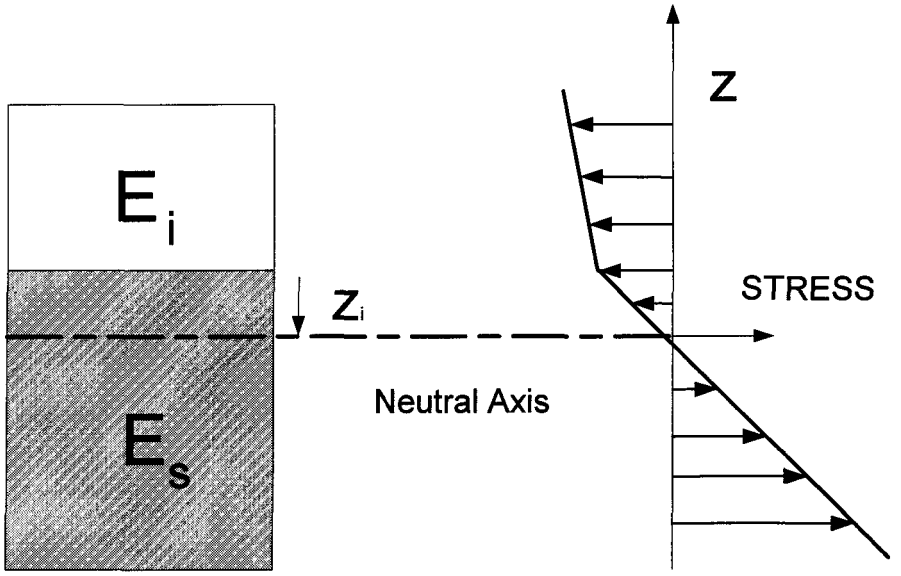

Figure 4.2: Bending stress repartition

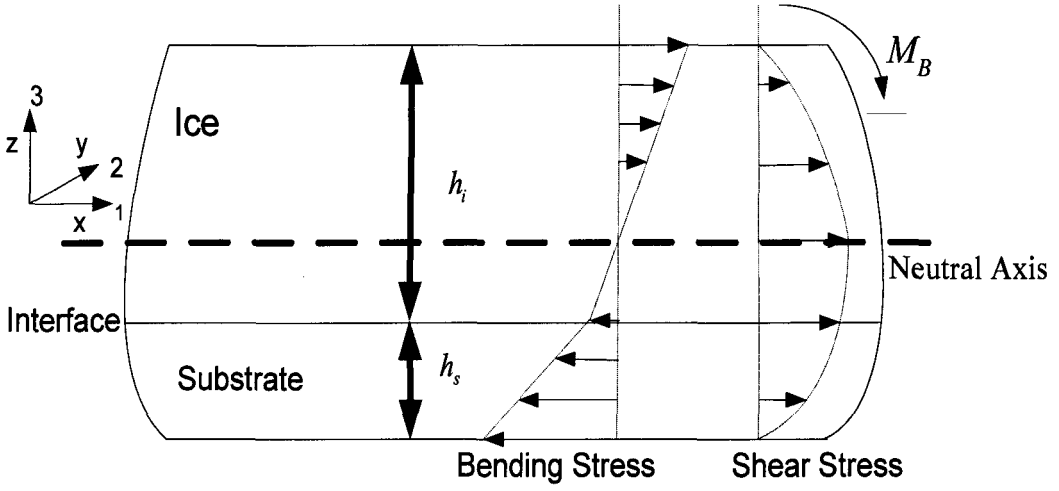

Figure 4.3: Aluminum/ice interface behavior under composite beam bending (applied case in tests)

4.2.2 Determination of Neutral Plane Position

When a beam is bent, one side narrows and the other side lengthens. Between the two, there is a neutral plane for which the bending stress is equal to zero and shear stress has its maximum value. The coordinate origin, the x axis, must be located at the neutral plane position in order to have the right value of z for calculating both bending and shear stress. The neutral plane position can be calculated using the moment equilibrium of the structure. It is carried out by calculating the stress in a cross section of the bimorph. The neutral plane is located at an unknown distance z_i from the interface as it is showed in Figure 4.2. In each material, the bending stress variation versus the z coordinate is linear and the element equilibrium requires the sum of normal forces to go to zero [29],

$$F_x = \int T_x dA = 0 \qquad \text{Eq.4.1}$$

where T_x is the bending stress. Considering a section made of two different materials with Young's modulus E_i and E_s as shown in Figure 4.2, then

$$\int_{-z_B}^{z_i} T_{ix} dA + \int_{z_i}^{z_T} T_{sx} dA = 0 \qquad \text{Eq.4.2}$$

Since $T_x = -\frac{Mz}{I}$, by consideration $|z|_{\max} = c$ we have, $T_x = T_{\max}\frac{z}{c}$ by substituting in above equation,

$$E_i \int_{-z_B}^{z_i} (\frac{z}{c} S_{\max}) dA + E_s \int_{z_i}^{z_T} (\frac{z}{c} S_{\max}) dA = 0 \qquad \text{Eq.4.3}$$

where $S_{\max}$ is the maximum strain at surfaces as shown in Figure 4.2 E_i and E_s are the Young's modulus of ice and substrate. After simplification,

$$z_B^2 = (1 - E_s / E_i) z_i^2 + (E_s / E_i) z_T^2 \qquad \text{Eq.4.4}$$

Depending on ice thickness the neutral axis can be located within ice or substrate. This discrepancy is well shown in Figures 4.2 and 4.3. Assuming the neutral axis is located within the ice (as in experimental test, Figure 4.3); the ice and substrate thicknesses are known, then substitution of $z_B = h_s + z_i$ and $z_T = h_i - z_i$ in Eq.4.4 gives,

$$z_i = \frac{h_s^2 - (E_s / E_i) h_i^2}{2h_s + 2(E_s / E_i) h_i} \qquad \text{Eq.4.5}$$

where h_i is ice thickness and h_s is substrate thickness. Subscripts B and T refer to bottom and top of the composite beam, respectively. If the obtained value for z_i is negative, it means that the NA is located in substrate. As it was expected in the case of having one material the NA is located at the mid plane. The coordinate origin, z axis will now be located at distance z_i from the ice/material interface.

4.2.3 Determination of Deflection (Bending Displacement)

In order to calibrate the Piezo film response a numerical model for our particular set-up was developed for studying the dynamic behavior of an aluminum beam, without ice, subjected to sinusoidal displacement. The neutral axis in this case is located at the middle thickness of the aluminum beam. Assuming that along the beam, the elastic modulus, inertia, and cross section area are constant and there is no ice deposition- for calibration of the Piezo response, there is no need for presence of ice as shown in Figure 4.4. A sinusoidal displacement $d = d_0 \cos(\omega t)$ is applied at the clamped end of beam. Assuming that the beam undergoes small deflections in the linearly elastic region, and has a uniform cross-section then the differential equation of motion for the bending displacement of the beam is known and is described later. Rotary inertia effects have not been considered. The bending displacement is obtained from the moment equilibrium in the structure. Assuming the deformation to be small enough such that the shear deformation is much smaller than bending displacement, $w(x,t)$, i.e., so that the sides of the element dx do not bend. This

planar beam, i.e., where all forces are exerted in the same plane, is a system of two internal stress components, shear and bending stresses.

According to Euler-Bernoulli Beam theory for a beam subjected to a transverse vibration[11] the differential equation of motion for the bending displacement of the beam is given by [30][31][32][33],

$$EI\frac{\partial^4 w(x,t)}{\partial x^4}+\rho A\frac{\partial^2 w(x,t)}{\partial t^2}=f(x,t) \qquad \text{Eq.4.6}$$

where E is the Young's modulus, I is the second moment of area of the beam cross section about the neutral axis (EI is so-called flexural rigidity), $w(x,t)$[12]is deflection of the structure, ρ is the mass density of the beam, A is the cross section area of the aluminum beam, and $f(x,t)$ is the external lateral force per unit length [34]. A separation of variables is assumed of the form $w(x,t)=W(x)\theta(t)$ where the solution of spatial equation is $W(x)$ and $\theta(t)$ is the solution of temporal equation [33].

[11] Transverse Vibration: vibration of the beam in the direction perpendicular to its length

[12] For this modeling, two important assumptions are made. First the beam thickness is supposed to be very small compared to its length, so that strain and stress along the 3-axis are equal to zero. Second, the structure width is assumed small compared to its length, hence strain and stress along the 2-direction is also equal to zero. So the bending displacement or deflection $w(x,y,z,t)$ reduces to $w(x,t)$.

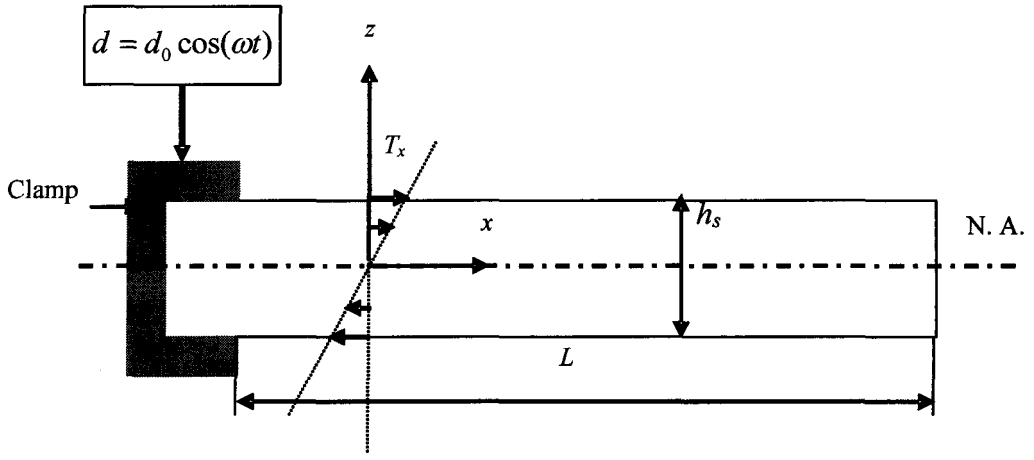

Figure 4.4: Aluminum clamped-free beam

The solution of temporal equation gives,

$$\theta(t) = \theta_1 \cos(\gamma t) + \theta_2 \sin(\gamma t) \qquad \text{Eq.4.7}$$

where the γ is the pulsation. The coefficients θ_1 and θ_2 can be calculated only if two initial conditions (initial deflection and velocity) are specified. In this study we do not need to have the temporal answer.

The homogeneous spatial equation comes [32],

$$EI \frac{d^4 W(x)}{dx^4} - \rho A \omega^2 W(x) = 0 \qquad \text{Eq.4.8}$$

$$\frac{d^4 W}{dx^4} - \beta^4 W = 0 \qquad \text{Eq.4.9}$$

where β is the flexural wave number given by

$$\beta^4 = \rho A \omega^2 / EI \qquad \text{Eq.4.10}$$

The general solution to Eq.4.9 leads to,

$$W(x) = k_1 \cosh \beta x + k_2 \sinh \beta x + k_3 \cos \beta x + k_4 \sin \beta x \qquad \text{Eq.4.11}$$

where the coefficients k_1, k_2, k_3, k_4 are determined using four boundary conditions of cantilever beam as follows:

- At clamped end, the deflection is equal to d_0 and its first derivative is equal to zero

$$W(x) = d_o \quad at \quad x = 0$$

$$\frac{dW(x)}{dx} = 0 \quad at \quad x = 0 \qquad \text{Eq.4.12}$$

By means of accelerometer, which is fixed at the clamed end of the set-up, the acceleration of the forced end is measurable, therefore for a given frequency, maximum displacement d_0 at the clamped end is known as,

$$d_0 = a / \omega^2 \qquad \text{Eq.4.13}$$

where a is acceleration expressed in (m/s^2), and ω in (rad/s).

- At the free end, the bending moment and the transverse shearing force are equal to zero.

$$EI\frac{d^2W(x)}{dx^2}=0 \quad at \quad x=L$$
$$EI\frac{d^3W(x)}{dx^3}=0 \quad at \quad x=L \qquad \text{Eq.4.14}$$

Finally, making use of boundary conditions, four coefficients of bending displacement are determined as:

$$k_1=\frac{d_0\cos\beta L-k_2.A_1}{A_2} \qquad \text{Eq.4.15}$$

$$k_2=\frac{d_0.(A_3\cos\beta L+A_2\sin\beta L)}{A_1A_3-A_2^{\,2}}$$

$$k_3=d_0-k_1$$

$$k_4=-k_2$$

where the three coefficients A_1, A_2, A_3 are given as,

$$A_1=\sin\beta L+\sinh\beta L \qquad \text{Eq.4.16}$$

$$A_2=\cos\beta L+\cosh\beta L$$

$$A_3=\sinh\beta L-\sin\beta L$$

In order to calibrate the Piezo film response we should calculate the stress induced at the aluminium beam surface. When there is no ice on the beam, the neutral axis is located at

the middle thickness of the aluminium beam $z_i = \frac{h_s}{2}$, thus shear stress at the surface is equal to zero while bending stress is equal to zero at neutral axis and it increases linearly to a maximum at the surface.

4.2.4 Determination of Bending Stress in order to Calibrate the Piezo Film Response

By knowing the functionality of bending displacement along 1-direction or x, it is possible to calculate bending stress on the surface of the aluminium beam as a function of bending moment. Thus, the following equation can be used [34],

$$T_x = \frac{M_B}{I} z \qquad \text{Eq.4.17}$$

where M is the bending moment, I is the area moment of inertia about the z axis, and z is distance from the neutral axis. The bending moment is the result of bending stress of structure and is given by [29],

$$M = -\int z T_x dA \qquad \text{Eq.4.18}$$

According to primary assumptions and simplification of Hook's law, the longitudinal stress is given by,

$$T_x = -\frac{E}{1-\nu^2}\varepsilon_x \qquad \text{Eq.4.19}$$

where ν is Poisson' s ratio, E is the Young modulus, and ε_x is the longitudinal strain. For such a cantilever beam the longitudinal strain is expressed as [29],

$$\varepsilon_x = -z\frac{d^2W}{dx^2} \qquad \text{Eq.4.20}$$

Substitution of Eq.4.20 into Eq.4.19 yields,

$$T_x = -\frac{E}{1-\nu^2}z\frac{d^2W}{dx^2} \qquad \text{Eq.4.21}$$

According to Euler-Bernoulli beam theory, bending moment as a function of bending displacement is given by,

$$M_B = -EI\frac{d^2W(x)}{dx^2} \qquad \text{Eq.4.22}$$

Eq.4.22 expresses bending moment as a function of deflection, $W(x)$. Substituting this equation in Eq.4.17, and considering $z = \frac{h_s}{2}$ (h_s is the thickness of the beam) results,

$$T_x = -E \frac{d^2W(x)}{dx^2} \frac{h_s}{2} \qquad \text{Eq.4.23}$$

Note, here the denominator $1-\nu^2$ in equation 4.21 is close to unity, since Poisson ratio of aluminium according to Table 4.2 is 0.33 then,

$$1-(0.33)^2 = 0.90 \cong 1$$

Thus bending stress as a function of bending displacement at the surface of the beam is obtained. Consequently, having beam dimensions, i.e., L, A ($A = b.h$, $I = \frac{bh^3}{12}$), its mass density ρ, and Young's modulus E, frequency and the acceleration at the clamped end, the exact theoretical value of bending stress induced at the surface along the beam is computable.

4.3 Calibration of Accelerometer

The output voltage of charge amplifier is

$$V' = k_{amp.} Q \qquad \text{Eq.4.24}$$

where $k_{amp.}$ is the amplification coefficient (gain of amplifier) which is calculated in this section for accelerometer calibration, V' is the output voltage of amplifier measured by means of an oscilloscope, and Q was measured by means of a charge amplifier type 4370 (Brûel & Kjaer Co.). Indeed this charge amplifier measures the acceleration in (ms^{-2}), then by multiplying this acceleration in accelerometer coefficient (transformation coefficient) that is 10.00 (pC / ms^{-2}), the resulted charge was obtained in (pC).

Moreover the Eq.4.24 can be shown as,

$$k_{amp.} = \frac{V'}{Q} \qquad \text{Eq.4.25}$$

By measuring the output voltage of amplifier and charge on accelerometer by means of a charge amplifier, the amplification coefficient (gain of amplifier) is calculated. In this study

considering the homemade piezoelectric film amplifier the value of amplification coefficient was $1.1*10^9$ (V/C).

4.4 Calibration of Piezo Film Response

The stress induced on the film can be expressed as,

$$T_1 = \frac{V_{out}}{K} \qquad \text{Eq.4.26}$$

where $K(Vm^2/N)$ is the adjusting coefficient in Data Acquisition Program which must be calculated for calibrating Piezoelectric film response, V_{out} is the output voltage[13] of the Piezo film after amplification measured by means of an oscilloscope (or Data Acquisition System during performing the tests with ice). Therefore for calibrating the Piezo film response, the adjusting coefficient, K, must be calculated. For this purpose consider Eq.3.3, which expresses Q as a function of Piezo film physical properties and induced stress,

$$Q = b.e.d_{31}.T_1 \qquad \text{Eq.4.27}$$

[13] Note that V' is the output voltage of amplifier itself without Piezo film where V_{out} is the output voltage[13] of the Piezo film after amplification, thus they are not equal

where b is the film width, e is the film length, as illustrated in Table 4.1, d_{31} is the piezoelectric coefficient (Piezo strain constant) with a value of $23*10^{-12}\frac{C/m^2}{N/m^2}$, and T_1 is the stress induced on the piezoelectric film.

Table.4.1: Dimensions of PVDF strip

	Tested Length or e (mm)	Width or b (mm)	Thickness (mm)
PVDF Strip	4	26	0.028

On the other hand it was seen in Eq.4.25 for accelerometer calibration that,

$$V' = k_{amp.}Q \Rightarrow Q = \frac{V'}{k_{amp.}} \qquad \text{Eq.4.28}$$

where $k_{amp.}$ is the amplification coefficient (gain of amplifier) with a value of $1.1*10^9$ (V/C) that was calculated for accelerometer calibration, V' is the output voltage of amplifier measured by means of an oscilloscope. Thereafter measured voltage is output voltage of Piezo film and Q is the charge induced on the film. Therefore stress induced on the film as a function of output voltage is given by,

$$T_1 = \frac{V_{out}}{k_{amp.}.b.e.d_{31}} = \frac{1}{K}V_{out} \qquad \text{Eq.4.29}$$

K is a known coefficient, thus the relation between the resulting stress T_1(Pa) and the output voltage of film, V_{out} (V), becomes:

$$T_1 = 0.38 * 10^6 * V_{out} \qquad \text{Eq.4.30}$$

Equation 4.30 was used to determine the magnitude of the stress at the location of the PVDF film; of course the known coefficient K was entered before into the Data acquisition program in order to calculate directly the induced stress during ice adhesion test.

4.5 Determination of adequate frequency exercised to electromagnetic shaker

As can be seen in Eq.4.10, β is a function of pulsation ω, which expresses the applied frequency of sinusoidal displacement $(\omega = 2\pi f)$. Hence determining the appropriate frequency for set-up is essential. According to theory in this set-up the first and second resonance frequencies were calculated as demonstrated in Eq.4.33 and Eq.4.34.

Table 4.2: Physical characteristics of the aluminum beam

Length (mm)	Width (b) (mm)	Thickness (h) (mm)	Young modulus (E) (GPa)	Poisson ratio (ν)	Mass density (ρ) (gr/cm^3)
280	25.4	3.1	66.8	0.33	2.712

I , which is the area moment of inertia about the z axis, by using Table 4.2 can be calculated as,

$$I = \frac{bh^3}{12} = \frac{25.4*10^{-3}*(3.1*10^{-3})^3}{12} = 63.05*10^{-12}(m^4) \qquad \text{Eq.4.31}$$

A, which is the cross section area of the aluminum beam, is given by,

$$A = b.h = 25.4*10^{-3}*3.1*10^{-3} = 78.74*10^{-6}(m^2) \qquad \text{Eq.4.32}$$

Therefore, the first and the second resonance frequencies of the aluminum beam are [34].

$$f_{1res} = \frac{1}{2\pi}(\frac{1.875}{L})^2\sqrt{\frac{EI}{\rho A}} = 31.64 \text{ Hz} \qquad \text{Eq.4.33}$$

$$f_{2res} = \frac{1}{2\pi}(\frac{4.6941}{L})^2\sqrt{\frac{EI}{\rho A}} = 198.41 \text{ Hz} \qquad \text{Eq.4.34}$$

Eq.4.23, $T_x = -E\frac{d^2W(x)}{dx^2}\frac{h_s}{2}$ expresses T as a function of $\frac{d^2W(x)}{dx^2}$, where $W(x)$ is given by Eq.4.11, which depends on $\beta, k_i (i = 1,2,3,4)$, and x. In addition according to Eq.4.10 β is a function of ω or applied frequency f ($\omega = 2\pi f$). Considering Eq.4.15 which expresses k_i coefficients as functions of d_0, maximum displacement,

$$k_1 = \frac{d_0 \cos\beta L - k_2 . A_1}{A_2}, k_2 = \frac{d_0 (A_3 \cos\beta L + A_2 \sin\beta L)}{A_1 A_3 - A_2^2}, k_3 = d_0 - k_1, k_4 = -k_2$$

Because of $d_0 = a/\omega^2$, $W(x)$ is a function of acceleration, too. In conclusion the bending stress is a function of applied frequency, acceleration as well as position. Figure 4.5 depicts bending stress as a function of frequency, for a given position (30 mm from the clamped end) and for a constant acceleration ($10 m.s^{-2}$).

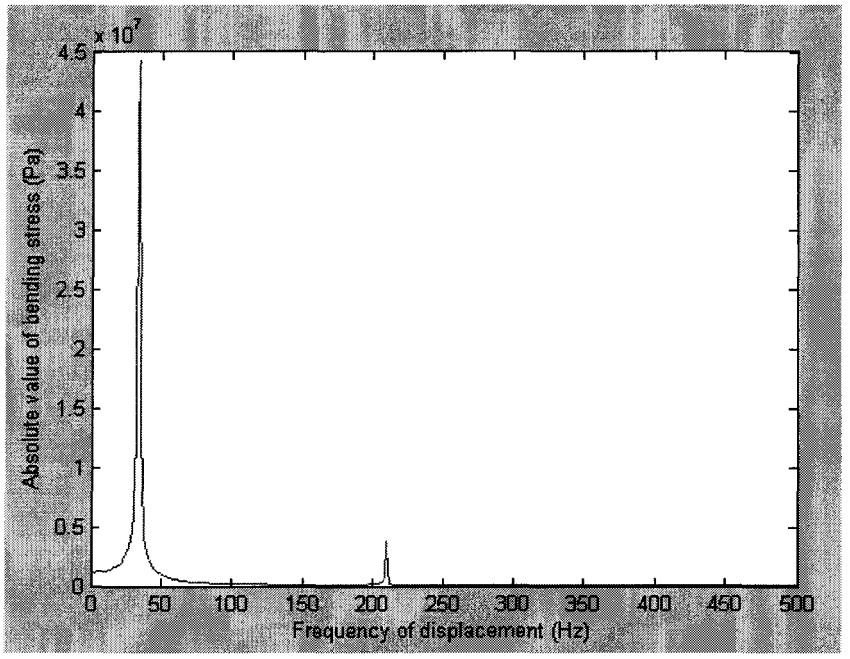

Figure 4.5: Bending stress as a function of frequency, for a given position and acceleration

It can be seen that maximum bending stress appears at first resonance frequency. Indeed bending stress, at the first resonance frequency, has the same order as ice adhesion strength in literature [4]. Therefore it seems more interesting selecting and working around first resonance frequency of the beam, between 30-34 Hz.

For more assurance, we illustrate bending stress as a function of position along the beam, for a given acceleration ($10 m.s^{-2}$) and the supposed frequency (30 Hz).

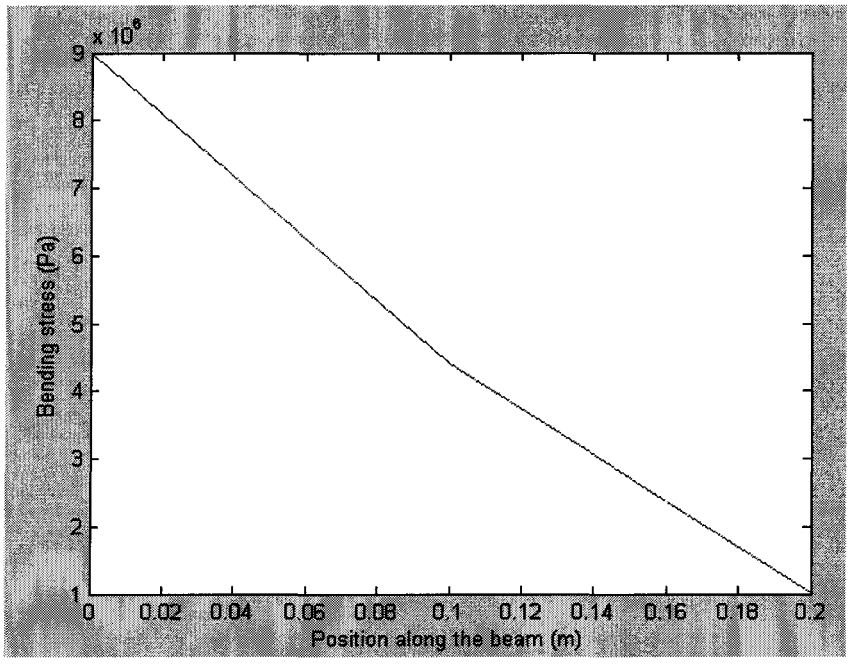

Figure 4.6: Bending stress as a function of position, for a given frequency and acceleration

Figure 4.6 shows the functionality of bending stress along the beam at 30 Hz. In fact bending stress, about frequency of 30 Hz, has the same order as ice adhesion strength in literature [4]. Figure 4.6 also shows that at low frequency, the distribution of bending stress is approximately linear and the maximum stress value is obtained at the clamped end.

It is more attractive working close to the first resonance frequency of the beam in order to induce the maximum resulting stress at the ice/aluminium interface. Moreover, adhesion failure should be initially induced much closer to the clamped end of the aluminium beam, where the stress has its maximum value. Consequently, the frequency of sinusoidal displacement is appropriately chosen close to the first resonance frequency, it means 30 Hz. Figure 4.6 reveals it is preferable that the PVDF film sensor be located close to the clamped

end of the beam (30 mm) because the bending stress increases by approaching to clamped end while near the free end (see Figure 4.6), it is more likely that the bending stress do not be sufficient for ice detachment, thus the piezoelectric film may not pick up the detachment strength.

4.6 Theoretical Modeling of Bending and Shear Stress in Presence of Ice at Interface

4.6.1 Modeling of Bending Stress

Hereafter, theoretical calculations for determination of bending and shear stresses, in presence of atmospheric ice layer on the substrate, at ice/material interface are presented. Obviously the only way to be insured of having reasonable and feasible modeling is to compare the practical results with the theoretical superposition of bending and shear stresses at interface. Unfortunately any model, measurement or particular experimental equipments do not exist in order to measure the exact value of Young modulus and Poisson ratio of atmospheric ice which is certainly different from the ordinary ice. Indeed ordinary ice results from water solidified in low temperature. Surely its physical and mechanical characteristics differ from atmospheric ice which forms from precipitation in nature or spraying supercooled water droplets in laboratory tests.

However it seems interesting to study the theoretical approach since there is similar approach in composite materials [28]. The determination of neutral axis plane has yet explained in detail in section 4.2.2. In order to determine bending displacement (deflection) of bimorph, Eq.4.8 was renewal,

$$EI\frac{d^4W(x)}{dx^4} - \rho A\omega^2 W(x) = 0 \qquad \text{Eq.4.35}$$

where EI is the global flexural rigidity, which is given by [25], and ρ is the total density $\rho A = \rho_i bh_i + \rho_s bh_s$ where ρ_i and ρ_s are ice and substrate densities, respectively, and A is the cross section area, $A = b*(h_i + h_s)$. The next step is determining the bending moment of the bimorph, referring to Eq.4.18 and Eq.4.21,

$$T_x = -\frac{E}{1-\nu^2} z_i \frac{d^2W}{dx^2} \qquad \text{Eq.4.36}$$

Note this equation is not apparently equal to Eq.4.23 which is obtained in order to calibrate the set-up without ice. Because in presence of ice the neutral plane is not located at aluminum midplane, z_i is given by Eq.4.5. In addition in theoretical analysis the denominator is maintained. For the case of a section made of two different materials as shown in Figure 4.7, the integral is divided into two parts, one for each elastic material

$$M = -\frac{d^2W}{dx^2}\left[\frac{E_i}{1-\nu_i^{\,2}}\left(\int_0^L\int_{z_B}^{z_i} z^2 dA\right) + \frac{E_s}{1-\nu_s^{\,2}}\left(\int_0^L\int_{z_i}^{z_T} z^2 dA\right)\right] \qquad \text{Eq.4.37}$$

where ν_i and ν_s are Poisson's ratio of ice and substrate, E_i and E_s are Ice and substrate Young modulus, respectively. The terms inside the parentheses represent the moment of inertia of the section about the neutral axis,

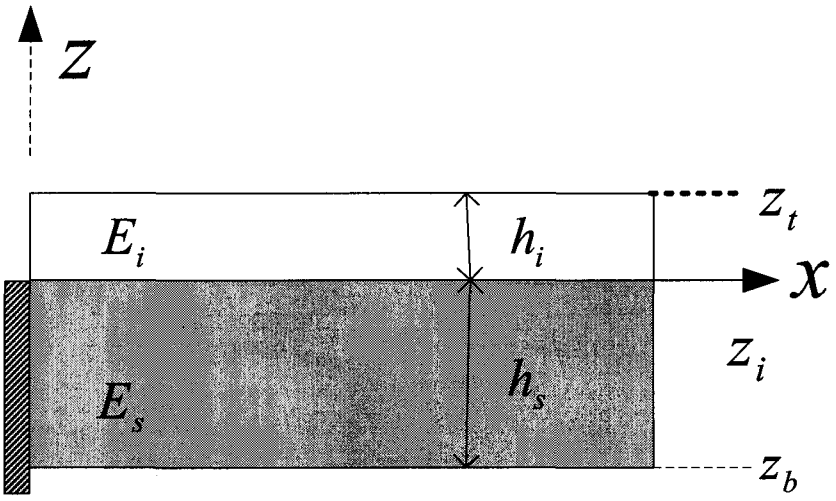

Figure 4.7: Coordinates of modeling, z_i demonstrates the neutral axis position

The global bending moment is,

$$M = -\frac{d^2W}{dx^2}\left[\frac{E_i I_i}{1-\nu_i^{\,2}} + \frac{E_s I_s}{1-\nu_s^{\,2}}\right] \qquad \text{Eq.4.38}$$

The previous relation can be seen from Euler-Bernoulli Beam Theory [34],which expresses bending moment as a function of deflection. The global bending moment can also be written as,

$$M_G = -EI\frac{d^2W}{dx^2} \qquad \text{Eq.4.39}$$

where EI is the global flexural rigidity of the structure,

$$EI = \frac{E_i I_i}{1-\nu_i^{\,2}} + \frac{E_s I_s}{1-\nu_s^{\,2}} \qquad \text{Eq.4.40}$$

Finally solving the moment equation for stress gives us the bending stress within the ice [33]

$$T_{xi} = -\frac{M_G}{I} z_i \qquad \text{Eq.4.41}$$

where M_G is the global bending moment, z_i is the distance from the neutral axis within the ice, and I is the moment of inertia of the section about the neutral axis of non-homogeneous beam which can be expressed as,

$$I = I_i + (E_s / E_i) I_s \qquad \text{Eq.4.42}$$

Substituting Eq.4.39 into Eq.4.41 gives the bending stress of ice as a function of bending displacement,

$$T_{xi} = -E\frac{d^2W}{dx^2}z_i \qquad \text{Eq.4.43}$$

The bending stress of the substrate is expressed as,

$$T_{xs} = -\frac{E_s}{E_i}\frac{M_G}{I}z_s \qquad \text{Eq.4.44}$$

where z_s is the distance from the neutral axis within the substrate.

4.6.2 Modeling of Shear stress

For this particular set-up, in addition to bending stress which develops in a loaded beam, e.g., ice covered beam there is also shear stress which develops at ice/substrate interface, including both a vertical shear stress and horizontal (longitudinal) shear stress. It can be shown that at any given point in the beam, the values of vertical shear stress and the horizontal shear stress must be equal at that point for static equilibrium [29]. As a result it is usual to discuss and calculate the horizontal shear stress in a beam. Thus, the formula for

the horizontal shear stress was derived. In this study, the value of shear stress was not considered for calibration; however it will be complementary to mention its related equations and calculations for a iced covered beam for having an idea about the values of horizontal and vertical shear stresses at interface, theoretically. It is remarkable that in this research the value of the contribution of both shear and bending stresses was simultaneously measured and no separation or distinction between two different stresses is practically possible.

Assuming the bimorph (aluminum beam and ice layer deposited on it) undergoes small deflections in the linearly elastic region, and has a uniform cross-section. According to Euler-Bernoulli Beam theory shear force can be expressed as the third derivative of transverse deflection,

$$\begin{cases} V = -EI\dfrac{\partial^3 w(x,t)}{\partial x^3} \\ w(x,t) = W(x)\theta(t) \end{cases} \Rightarrow \quad V = -EI\frac{d^3 W(x)}{dx^3} \qquad \text{Eq.4.45}$$

The shear stress τ generated from the shear force can now be calculated as [34][35],

$$\tau = \frac{VQ^*}{Ib} \qquad \text{Eq.4.46}$$

where Q^* is the first moment of the area about the neutral axis. For composite areas, i.e.,

ice and substrate, the first moment of area can be calculated for each part and then added together. The equation for Q in this case is

$$Q^* = \sum A_j^* z_{c_j^*} \qquad \text{Eq.4.47}$$

where A_j^* is the area of the part of the cross section that is considered, $z_{c_j^*}$ is the vertical distance from the centroid of the cross section to the centroid of A_j^* as shown in Figure 4.8 and I is the moment of inertia of the section about the neutral axis.

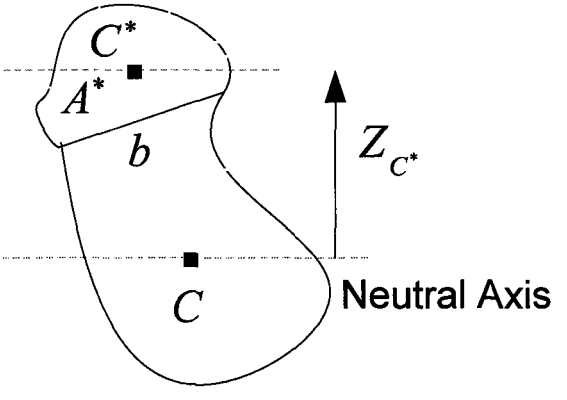

Figure 4.8: z_{c^*} is the vertical distance from the centroid of the cross section to the centroid of A* [29]

Substituting Eq.4.45 in Eq.4.46 gives the shear stress as a function of bending displacement,

$$\tau = -E\frac{Q^*}{b}\frac{d^3W}{dx^3} \qquad \text{Eq.4.48}$$

Assuming that before ice detachment, in the linearly elastic region, the displacement and the strain tensor are the same for both substrate and ice at interface, because they are closely linked.

It is remarkable that inertia forces of ice accretion are negligible in comparison with shear and bending forces acting at the interface. The bending displacement of the beam is very small, around 4 mm for the free extremity of the composite beam. The maximum inertia force due to the beam acceleration can be expressed as a function of the bending displacement as follow:

$$F_{i\max} = \int_0^L \frac{m}{L}(g + \frac{\partial^2 W(x,t)}{\partial t^2})dx \qquad \text{Eq.4.49}$$

where $W(x,t) = W(x).e^{i\omega t}$ is the bending displacement with $W(x)$ [14], which represents the spatial part of the bending displacement.

Hence, as $\frac{\partial^2 W(x,t)}{\partial t^2} = -\omega^2 W(x,t)$ and with a small ice masse m (around 28 g), the inertia force induced by the ice deposit is around 1.15 N. This correspond to a normal

[14] which will be described later

stress of 161 Pa applied to the center of gravity of ice deposit. In this context, the contribution of the inertia force of the acceleration of ice deposit in the process of ice de-bonding can be neglected in comparison of the range mentioned in literature [4] means about 0.2 MPa, required to ice de-bonding.

CHAPTER 5
EXPERIMENTAL SETUP, FACILITIES AND TESTS PROCEDURE

Chapter 5
Experimental Set-up, Facilities and Tests Procedure

5.1 Introduction

In order to achieve the objectives, an experimental study was systematically carried out in the laboratory of CIGELE/INGIVRE in Université du Québec à Chicoutimi. For this purpose, the atmospheric icing conditions were simulated by spraying super cooled water droplets on the prototypes. This chapter introduces laboratory facilities, the experimental set-up and the test procedure used in this particular technique of measuring ice adhesion strength.

5.2 Laboratory Facilities

5.2.1 Ice deposition in climate room

Scientific tests should be repeatable and comparable. Therefore, the tests were carried out in a chamber that makes it possible to control precisely the environmental conditions, such as temperature, wind velocity, and ice-thickness deposited on beams. In this study, all the adhesion tests were performed in one climate rooms at CIGELE that is equipped with a water droplet generator (nozzle) and a cooling system, which makes it possible to form an

ice layer on the surface of the beam. Then, beams were placed on a stand shown in Figure 5.1, with a constant slope angle of 47° and constant distance from the nozzle, inside the climatic chamber where exposed to atmospheric ice accretion obtained from spraying cooled water droplets under the experimental conditions presented in Table 5.1 In order to have isothermal conditions for beams in the chamber, they were exposed about two hours to dry air before beginning ice deposition.

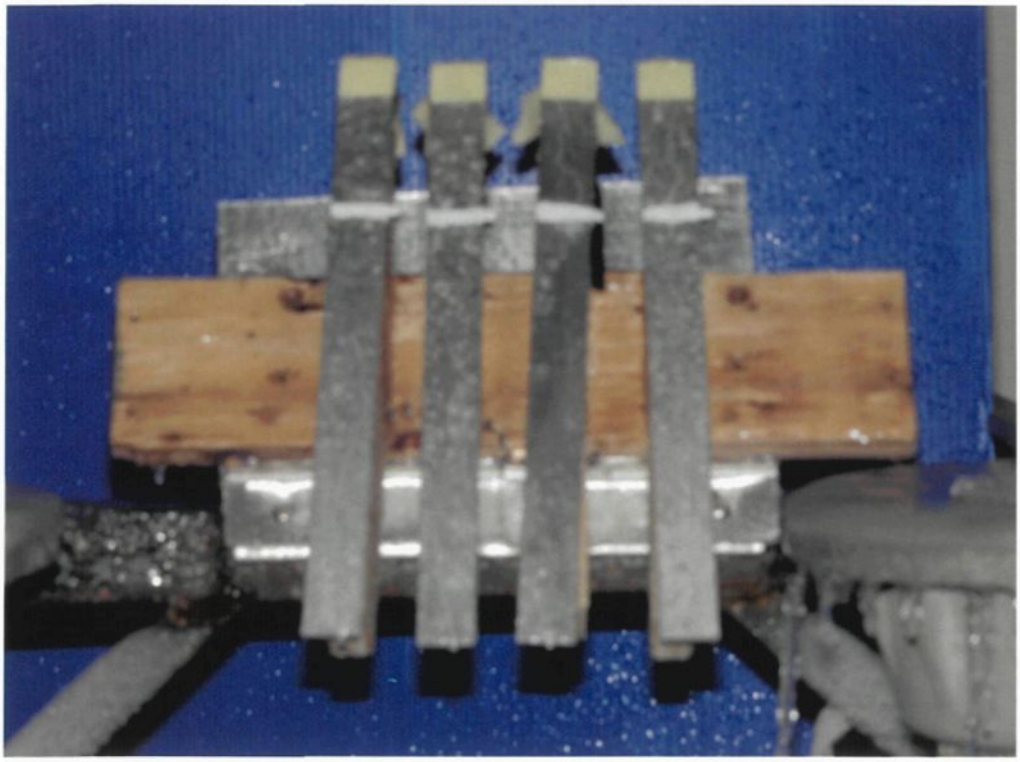

Figure 5.1: Beams placed on the stand exposed to artificial ice deposition

Table 5.1: Constant Parameters used for atmospheric ice accretion

Test Parameters	Parameters values
Air temperature (°C)	-12(± 0.2)
Freezing water temperature (°C)	3
Water droplet size (μm)	around 80
Precipitation rate (mm/hr)	18
Wind Speed (m/s)	3.3
Water Pressure (psi)	60
Ice thickness(mm)	3-4

5.2.2 Water droplet generator

The water droplet generator is comprised of an oscillating nozzle with 30 Hz frequency of oscillation, in all tests. The type of flat spray standard nozzle-*VeeJet spray nozzle with small capacity of 0.12 gallon per minute at 60 psi*-is H1/4VV2501 shown in Figure 5.2. It is located in front of the 1.5-meter-height stand with 1.9 meter horizontal distance and 2.9 meter height. The spray angle at 60 psi was set at 30° C.

As we all know, glaze adhesion is the most dangerous to the power systems; therefore glaze adhesion is more interesting to measure. For that reason by adjusting the water pressure fed into the nozzle to 60 psi, the water droplet size is adjusted to 80 μm in order to particularly have the glaze ice type. Wind velocity, as another important factor affecting the ice type, was set to 3.3m/s.

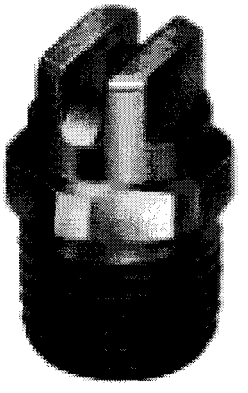

Figure5.2: Flat Spray Standard Nozzle, H1/4VV2501

5.2.3 Cooling system

To simulate cold atmospheric icing conditions, our laboratory is equipped with an ammonia cooling system. This system is made up of a compressor and computer-controlled regulators, which allow to very rapidly reach air temperatures as low as –30°C ± 0.2°C. The accuracy of temperature control is 0.1°C. In order to produce the glaze in this study, the environmental temperature was adjusted to -12°C during the ice accretion period. The

water conductivity was set to its minimum about 5-8 $\mu s / cm$ in order to minimize the probability of affecting charge induced on the piezoelectric film while tap water conductivity is about 80 $\mu s / cm$. The humidity of the room, which has an important role in ice adhesion value, was measured by a Hygro-Thermo anemometer (HHF710) as '81.6%'[15].

5.2.4 Data acquisition system

The test data, including the stress and acceleration were monitored and recorded by a data acquisition system, which consists of a PC-compatible, high-speed data acquisition card developed in MATLAB environment.

5.2.5 Glues

For this study, as shown in Figure 5.3, two kinds of glues were necessary;

- Insulated glue that was applied between piezoelectric film and aluminium beam
- Conductor glue that was applied between piezoelectric film and electrical wires

[15] This value shows relative humidity which defines as the percent of saturation humidity [38], R.H.= (actual vapor density/saturation vapor density) * 100. Saturation vapor density depends on temperature, for example in -10° C it is 2.36 gm/m^3

In order to have an insulated and vibration resistant contact a special epoxy, named EPOXY RESIN RBC # 3215, was used. Weighing the desired amount of resin and hardener into a clean container, mixing thoroughly and potting it in 60° C for 4 hour, gives the best result. It is remarkable that this epoxy bonds well to aluminium, polypropylene and glass and its operating temperature range is -55° to 100° C, thus applicable for many types of substrates and for icing condition.

Conductor glue, epoxy modelled EE129-4, makes an excellent electrical contact between two piezoelectric electrodes and electrical wires. Wires which were used here were insulated, varnished winding wires from copper. Their diameter was rather fine about 0.1 mm. It is remarkable that for each prepared prototype the contact resistance was checked in order to ensure that the electrical contacts are all right.

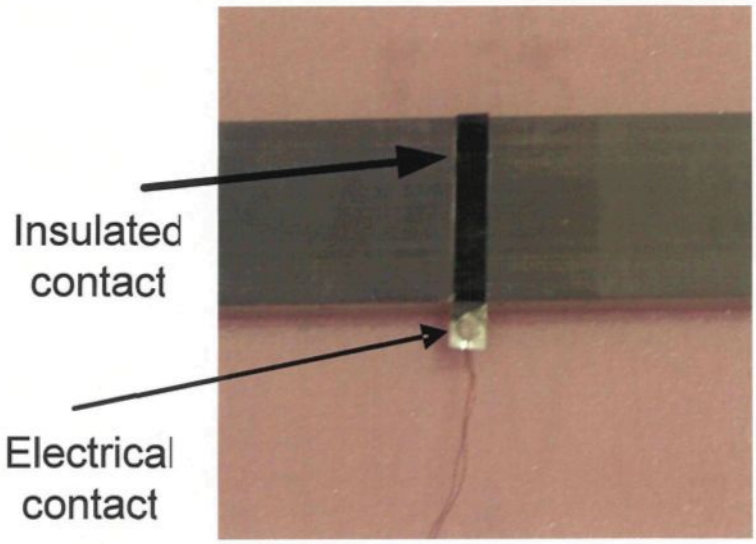

Figure 5.3: Practical exhibition of glues

5.2.6 Accelerometer

A charge accelerometer, type 4370 (Brûel & Kjaer Co.), is mounted on the clamped end in order to measure the acceleration of the beam during the test, however accelerometer is not principally used to measure acceleration but to determine the displacement of the clamped end, seen in Eq.4.13. The accelerometer was calibrated by a charge amplifier named "Measuring Amplifier Type 2525" made by Brûel & Kjaer. The accelerometer was used to calibrate the charge amplifier, too. Note that the amplitude of sinusoidal displacement was increased manually that is not ideal for having a good ramp. As one of future works, developing a software for automating of amplitude command seems necessary.

5.2.7 Aluminum Beam and Piezoelectric Film

The aluminum beam that was used in ice adhesion tests was 'Alcoa Alloy 6061-T6511'. Its general characteristics are excellent joining, good acceptance of applied coatings, combines relatively high strength, good workability and high resistance to corrosion. Transmission lines conductors are generally are made in two parts, core and conductor. The envelope wires are made from aluminum or copper. In the North America aluminum is a common material used for conductors. Its Young modulus $E = 66.8GPa$, its Poisson ratio, $\nu = 0.33$, its mass density $\rho = 2.712gr/cm^3$ are known exactly. In this study two different surface

finishes (roughness) was applied. The first series of prototypes were polished by aluminum oxide sandpaper no.180, following by a cleaning step using acetone. The second series were polished by sandpaper no.400 following by a cotton polishing wheel, in order to have a more finished surface. In Table 5.2 dimensions of both types of aluminum beams and also piezoelectric films glued on the aluminum surface, is given. The PVDF film used has a d_{31} charge coefficient value of 23.10^{-12} $((pc/m^2)/(N/m^2))$.

Table 5.2: Dimensions of the aluminum beam and PVDF strip

	Tested Length (mm)	Width (mm)	Thickness (mm)
Beam (no. 180)	280	25.4	3.1
Beam (no. 400)	280	25.4	3.1
PVDF Strip	4	26	0.028

5.2.8 Charge Amplifier Circuit

As shown in Figure 5.4 a homemade charge amplifier was prepared in order to cancel environmental noise and reinforce piezoelectric film signals. The charge amplifier gives a voltage output which is directly proportional to the charge induced on the piezoelectric

film. Hence, the output voltage of the charge amplifier is directly proportional to the resulting stress measured at the ice/aluminum interface. Amplifier input comes from piezoelectric film and accelerometer and its output goes to the data acquisition system and a PC in order to record simultaneously the total charge and acceleration in all the moments and then to calculate the stress induced on the beam by means of a special MATLAB Programming.

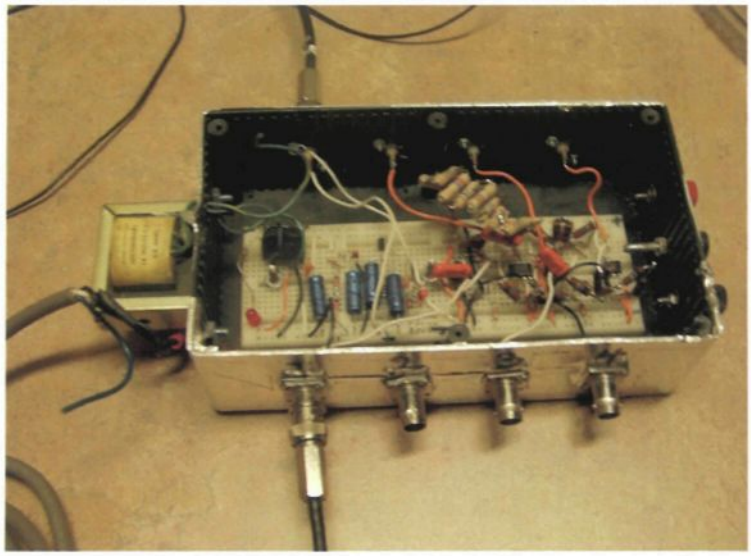

Figure5.4: Homemade Charge Amplifier

The transistor selected for this charge amplifier was low-power J-FET operational amplifier named as 'TL061CP'. It features high input impedance; wide bandwidth, high slew rate, and low input offset and input bias currents. Figure 5.5 illustrates top view of 'TL061CP' package.

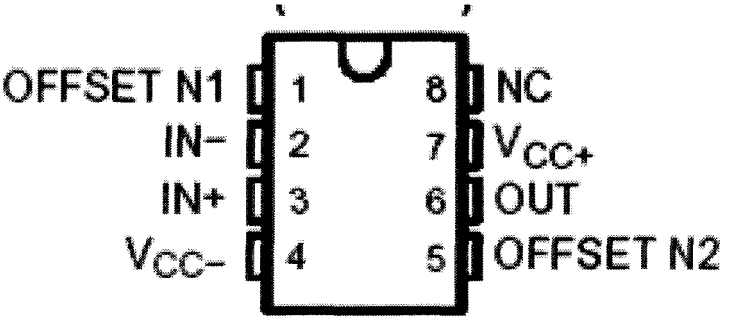

Figure5.5: Top view of 'TL061CP' package

Figure 5.6 shows the charge amplifier circuit used in this research. Note for each piezoelectric film an equivalent charge amplifier circuit is needed. Moreover a charge amplifier circuit was considered for accelerometer.

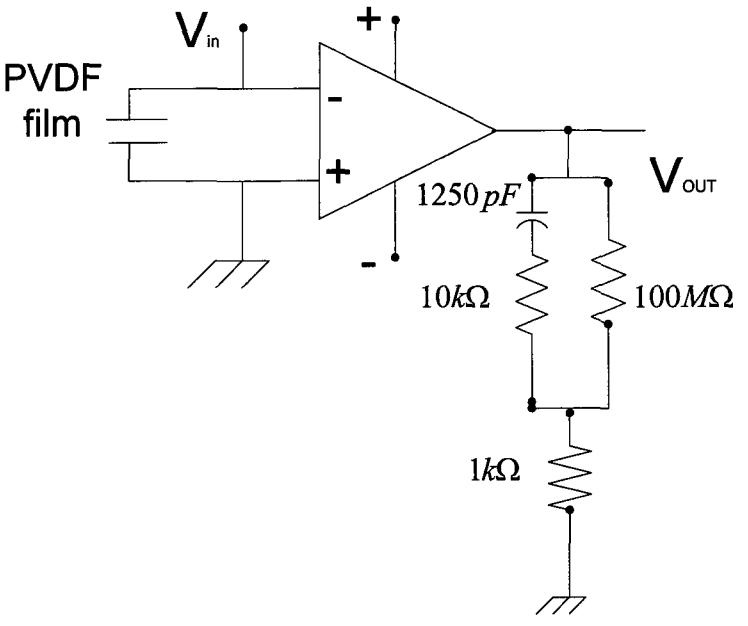

Figure 5.6: Schematic illustration of homemade charge amplifier

5.2.9 Beam preparation and icing

After carefully preparation of the surface of each sample beam, as described in section 5.2.7, aluminium beams were placed on a stand inside the climatic chamber at -12°C and exposed to atmospheric ice accretion obtained from spraying cooled water droplets under the experimental conditions presented in section 5.2.1.

The thickness of the ice on the aluminium beam was 4 mm of glaze ice, with a density of around 0.9 g/cm^3. Figure 8 shows the ice layer at the end of the ice accretion process. In

order to avoid a short circuit between the electrodes and the ice layer, a white electrical isolating layer was fixed on the PVDF film before ice accretion.

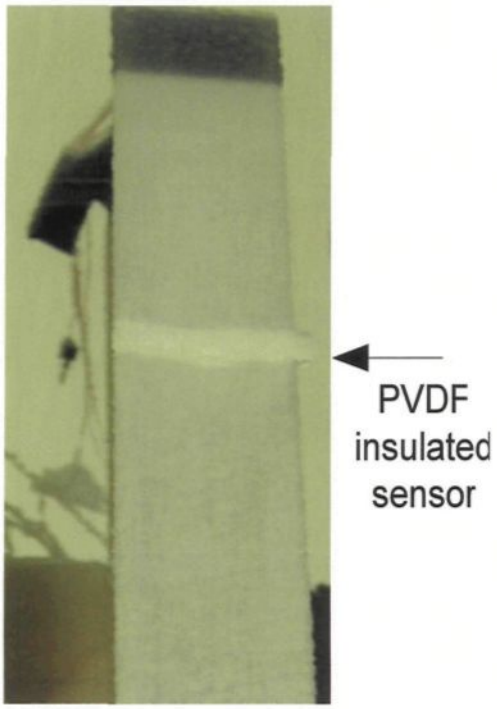

Figure 5.7: Ice layer obtained at the end of the atmospheric ice accretion process

5.3 Experimental Set-up

An electromagnetic shaker and frequency generator were used in order to induce the necessary sinusoidal displacement to the aluminium beam at the clamped end. Note ice is a brittle material, only the aluminum beam is clamped. Figure 5.8 shows the experimental setup of the method developed.

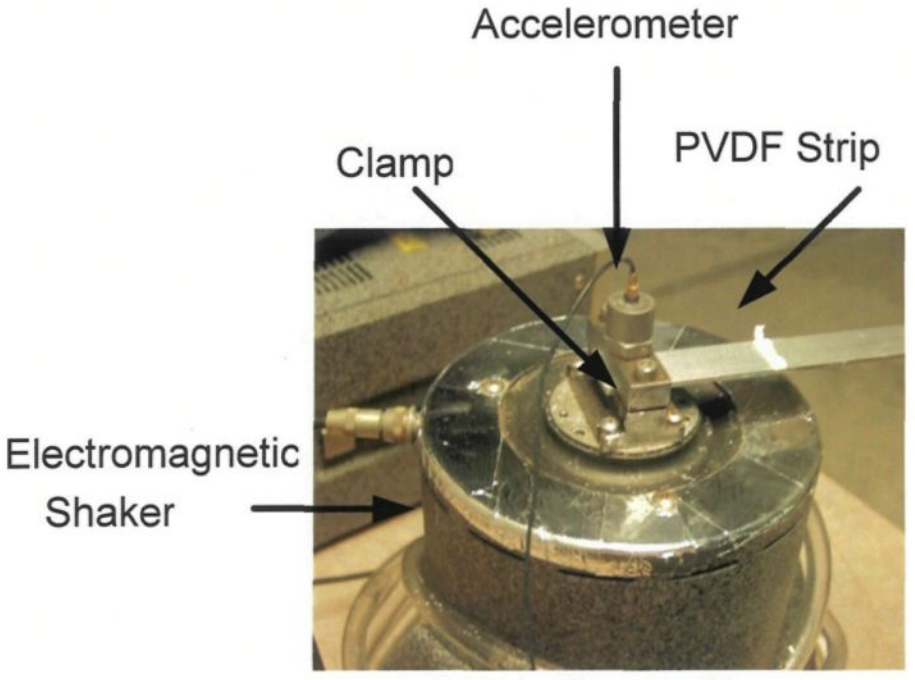

Figure 5.8: Experimental setup

The clamp is directly fixed to the moving part of the electromagnetic shaker in order to provide the sinusoidal normal displacement $d_0 \cos(\omega t)$ which is measured with the accelerometer fixed on the top of the clamp (see Figure 5.8). The PVDF strips bonded to the aluminum beam are larger than the beam width in order to properly carry out the electrical contact on the PVDF electrodes, as illustrated in Figure 5.8. This also ensures a rigid mechanical bond between the PVDF strips and the substrate.

5.4 Tests Procedure

Hereafter all the exact tests procedure is explained systematically. The calibrations of accelerometer and piezoelectric film had been performed before the tests commencement.

1. Prepared beams (finished beams with glued piezoelectric film) are weighed before icing.

2. Ice thickness is measured after icing.

3. Beams are weighed following icing in order to calculate ice density.

4. After icing, the composite beam is clamped onto the electromagnetic shaker inside the cold room.

5. The PVDF film sensor and accelerometer are connected to the Data Acquisition System (DAS).

6. The frequency of the electromagnetic shaker is set to 30Hz.

7. As explained before, for a frequency of about the resonance frequency of the structure (30 Hz for aluminum beam) and constantly increasing amplitude. Note that the strain rate must be suitable.
8. Afterwards the commencement of DAS recording, the amplitude of the displacement *d* is constantly and progressively increased from zero until the ice de-bonding.

9. Piezoelectric cells pick up the ice detachment force.

10. The collected data by Data Acquisition System contain the exact moment, and stress value of ice detachment with tracing the variation in received signals from the piezoelectric films during the test, as specimens shown in Figure 5.9 and Figure 5.10.

11. The results are analyzed in terms of surface roughness.

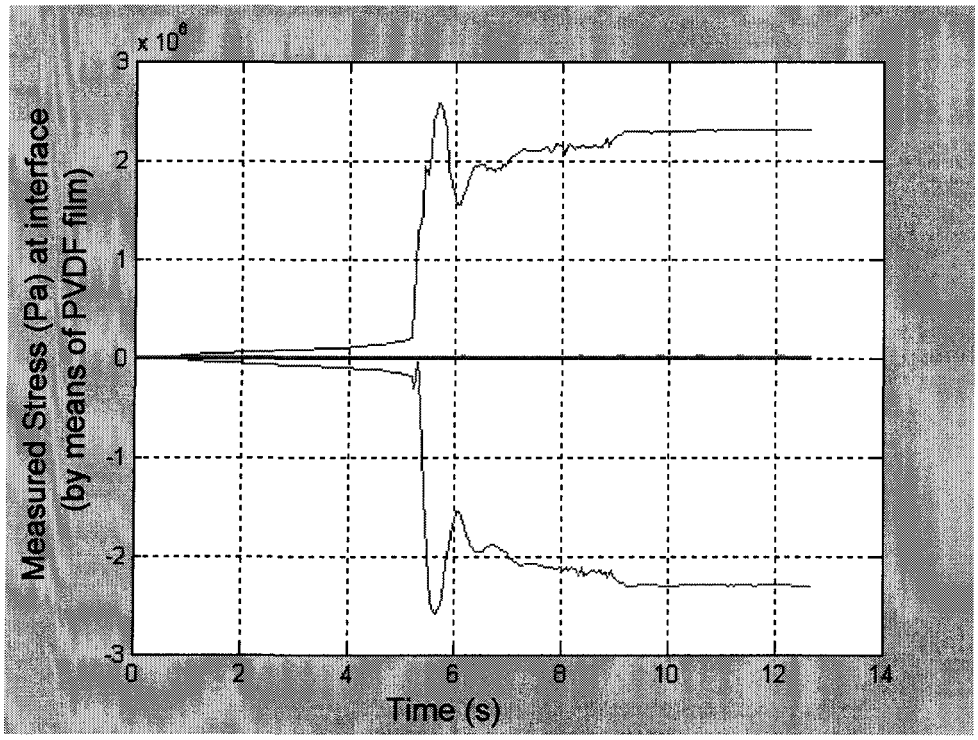

Figure5.9: Measured stress for Al (180)

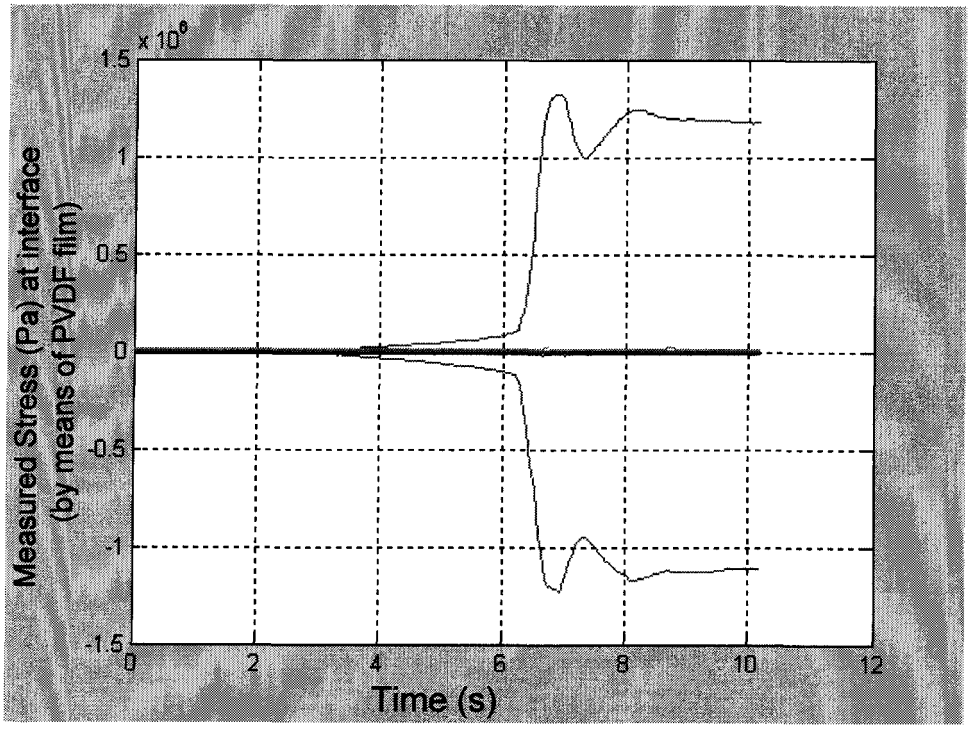

Figure5.7: Measured stress for Al (400)

In next chapter we will discuss more about the resulted graphs and the value obtained for ice adhesion strength.

CHAPTER 6
EXPERIMENTAL RESULTS

Chapter 6
Experimental results

1.1 Introduction

After the completion of many preliminary tests, a series of four tests were performed under the same conditions with a PVDF film sensor placed at 30 mm from the clamped end at a constant temperature of -12°C. The temporal evolution of the resulting stress measured by the PVDF film at the ice/aluminium interface is presented in Figure 6.1 and Figure 6.2. Each graph corresponds to the positive and negative envelope of the sinusoidal signal obtained from PVDF films. The results of Figure 6.1 show the evolution of the stress magnitude on the aluminium surface less finished (polished by sandpaper no.180) as measured by the PVDF film. Figure 6.2 demonstrates the stress magnitude on the aluminium surface more finished (polished by sandpaper no.400 following a cotton polishing wheel). Thus the experimental results were affected by surface roughness. The obtained empirically results demonstrate that ice adhesion strength depends on the surface finish, as it is more finished the adhesion strength is less, which can be explained by mechanical interlocking mechanism[16]. Evidently mechanical interlocking plays a more important role when a surface is less finished. It may be observed that, in all test series,

[16] Which is explained precisely in chapter 2

with an increase in the displacement amplitude of the clamped end, the interface stress increases quite linearly until delamination or ice de-bonding occurs at the film position. At this specific moment a drastic change in the interface stress occurred resulting from a local redistribution of the bending and shear stress. Hence, the interface stress obtained at this specific moment corresponds to the stress needed to de-bond the ice from its substrate (ice adhesion strength). The ice adherence force obtained for each test series are presented in Table 6.1.

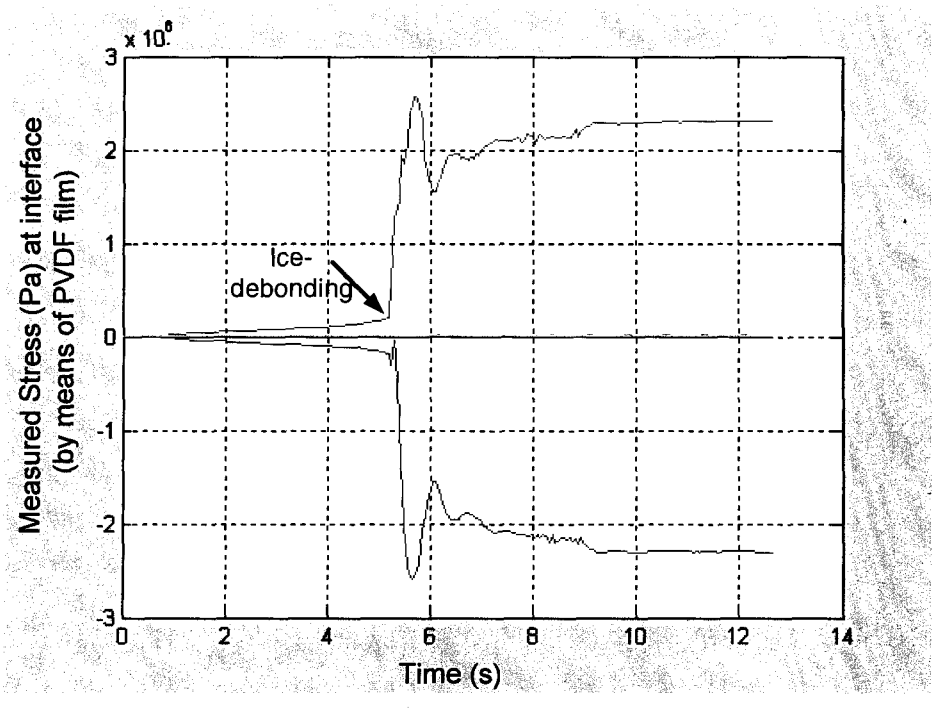

Figure 6.1: Temporal evolution of the resulting ice/aluminum interface stress obtained from the PVDF embedded sensor (finished AL 180)

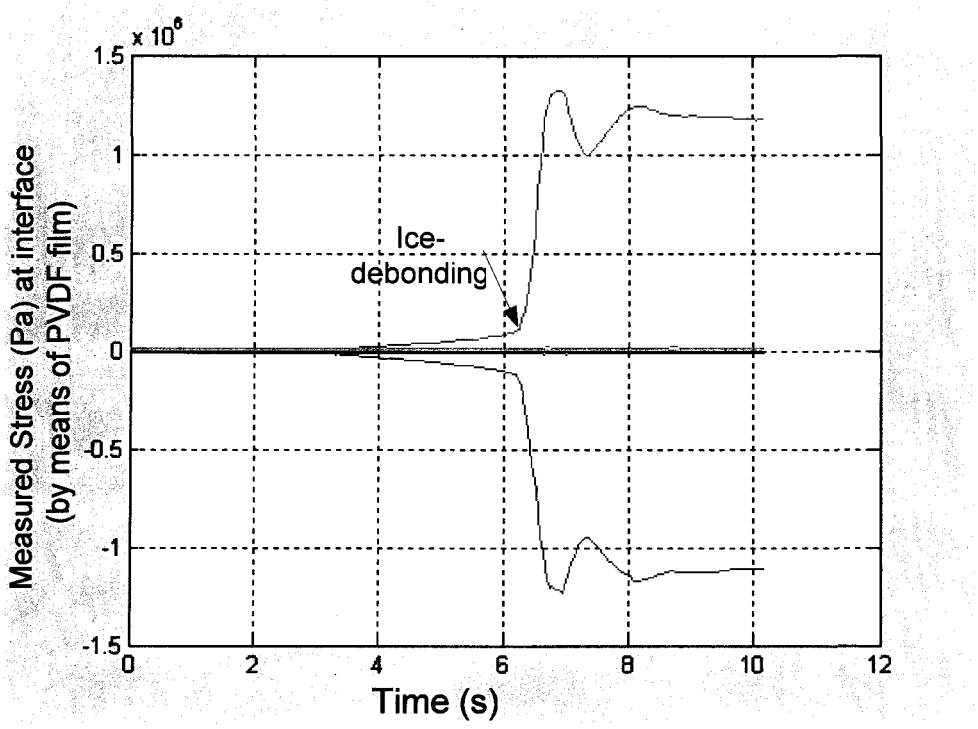

Figure 6.2: Temporal evolution of the resulting ice/aluminum interface stress obtained from the PVDF embedded sensor (finished AL 400)

In the Table 6.1 the resulting interface stress in MPa are expressed for Aluminium finished by sand paper no.180 and 400 and Plexiglas. The same method, technique and constraints have been used for carrying out tests using Plexiglas. The obtained empirically results demonstrate that ice adhesion strength depends on the surface finish. Otherwise the adhesion strength increases when the substrate surface roughness is increased. As can be seen in Table 6.1, the experimental results prove that ice adhesion strength depends significantly on substrate type as the adhesion strength on Plexiglas surface was 100 times less than on the aluminum surface. This can be explained that electrostatic attractions

between ice/Plexiglas are significantly less than ice/Aluminum. The Plexiglas surface is also more finished than the aluminum surface.

Table 6.1: Ice Adhesion test results

	Position of the PVDF film from the clamp (mm)	Resulting Interface stress (MPa) AL Beam Roughness(400)	Resulting Interface stress (MPa) AL Beam Roughness (180)	Resulting Interface stress (MPa) Plexiglas
Beam #1	28	1.2	2.5	0.04
Beam #2	28	1.5	2.6	0.03
Beam #3	28	1.7	3.0	0.06
Beam #4	28	1.6	2.9	0.08
Beam #5	28	1.4	2.8	0.04
Beam #6	28	1.7	3.2	0.06
Mean value of measured stress	----------	1.5 ± 0.06	2.8 ± 0.09	0.05 ± 0.002

On the basis of the results of Table 6.1, the mean value obtained for the adhesive strength of the ice on aluminium finished by sand paper no.400 was, 1.5 ± 0.06 MPa on aluminium finished by sand paper no.180 were 2.8 ± 0.09 MPa, and on Plexiglas was 0.0515 ± 0.215

On the basis of the results of Table 6.1, the mean value obtained for the adhesive strength of the ice on aluminium finished by sand paper no.400 was, 1.5 ± 0.06 MPa on aluminium finished by sand paper no.180 were 2.8 ± 0.09 MPa, and on Plexiglas was 0.0515 ± 0.215 MPa. These results are in the same order of magnitude as those reported in literature review as 0.2 MPa to 2 MPa or as results found for shear adhesive strength reported in literature which varies from 0.2 MPa to 1.0 MPa [13]. This value is the result of the contribution of the bending and shear forces generated at the ice/beam interface due to clamped end's sinusoidal displacement.

Before conducting the ice adhesion measurement, several preliminary tests were performed with different ice thicknesses, at constant temperature of -10°C. These tests verified if adhesive failure was definitely obtained at the previously determined frequency. In particular for each test, as the amplitude of the sinusoidal displacement increased, ice was observed to detach itself from the beam starting at the clamped end and propagating along the beam with the increase of *d*. In many cases, the propagation of this ice de-bonding or delamination occurred without any visual crack until it reached about at the middle length of the beam[17]. At this moment, many cracks perpendicular to the beam length were produced, leading to ice shedding from the beam.

One of the main advantages of this experimental set-up is that this technique is not confined by the thickness of the ice or substrate nor by the position of the neutral axis, as in

[17] However this is not exactly measured

the case of the presented in the last technique in review of literature [4]. This particular condition was used in the ice adhesion measurement method developed by [4] based on the flexion of an ice/composite substrate beam. In the latter method, ice thickness is chosen in order to induce the maximum value of shear stress at the interface which is indirectly deduced from measuring the applied force and beam displacement. This technique is very sensible to neutral axis position consequently it is very sensible to ice thickness, it means by a little and unwanted change of ice thickness, the measurement is not reliable.

From Figure 6.3 and Figure 6.4, it can be observed that the magnitude of the stress at the aluminium/ice interface is directly linked with the position of the neutral axis (N.A.) and, consequently, the magnitude of stress induced at the interface depends directly on the thickness of the ice layer and substrate. Along the neutral axis the bending stress is equal to zero whereas the shear stress is maximum. As it is shown in Figure 6.3[18] when the neutral axis is located within the ice, the bending stress direction is not the same as that of the shear stress at the aluminium/ice interface. Similarly from Figure 6.4 it is remarkable that when the neutral axis placed within the substrate the direction of bending stress is the same as that of the shear stress; however they are never in the same plane. Note as mentioned before shear stress and bending stress do not act in the same plane, however paying attention to the vector direction of shear and bending stresses is more tangible. However it does not mean that for all different ice or substrate thicknesses the magnitude of the stress induced at the interface is the same. The magnitude of stress at the interface has different

[18] For more clearance both of the figures are shown at the same page (111).

values depending on the ice and substrate thicknesses [4]. Although in present study a comparison between the two possibilities shown in Figure 6.3 and Figure 6.4 have not been done. In this study the configuration of Figure 6.3 is tested since the aluminium beam thickness is 3.1 mm and the deposited ice thickness is 4mm.Apparently using Table 4.2 and Eq.4.5 yields the neutral axis position in this set-up. However knowing the exact Young modulus of artificially deposited atmospheric ice seems necessary for obtaining more precise result. It would be a great interest as a future work to study the influence of ice and substrate thicknesses in experimental results (the variation of stress induced at the interface).

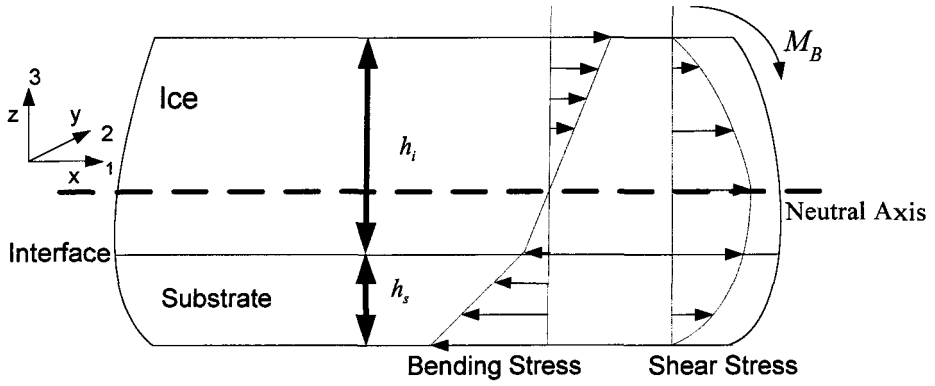

Figure 6.3: Induced stress distribution at interface as the contribution of both shear and bending stresses, when ice is thicker

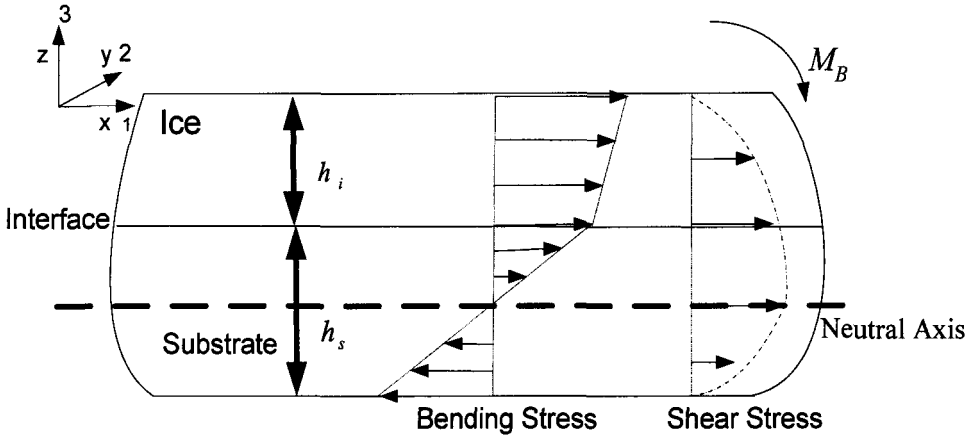

Figure 6.4: Induced stress distribution at interface as the contribution of both shear and bending stresses, when substrate is thicker

CHAPTER 7
CONCLUSIONS AND RECOMMENDATIONS

Chapter 7
Conclusions and Recommendations

7.1 Conclusions

As demonstrated in previous six chapters, this study was dedicated to introduce a new mechanical, macroscopic and direct technique for estimating atmospheric ice adhesion strength on structures. The great advantages of the proposed method compared to existing methods can be enumerated as follows,

1 The apparatus was designed using the principle of a Cantilever Beam

2 The increasing rate of applied load is not instantaneous as exist in 'impact test'.

3 The load is applied directly on substrate surface not directly on the ice which has a brittle structure, contrary to many techniques mentioned in chapter 2 as 'cylinder torsion shear tests' or 'axial cylinder shear test'.

4 This technique can quantify the adhesion strength of very thin ice layers, too.

5 The adhesion strength can be quantified directly. Almost all techniques reviewed in chapter 2 quantify the value of adhesion force indirectly, which increases the probability of errors and decreases the certitude of the result.

6 The presented technique is applicable for atmospheric ice which has completely different characteristics as well as structure from the ordinary ice.

7 Laboratory observations revealed that in all performed tests failures occurred on the beam, were 'adhesive failure' that is desired in adhesion tests.

8 In order that the increasing rate of applied load is not instantaneous, the failure is not instantaneous, too. The Propagation of ice delamination starts from the clamped end to the free end gradually by appearance of cracks along the prototype. This progression is even visible by naked eyes as a color change of ice.

9 The method makes it possible to measure the contribution of both shear and bending stresses anywhere along the beam.

10 The technique can be carried out on various types of substrate by adjusting all proper parameters, provided their mechanical properties are known.

11 The originality of the study is application of Piezoelectric Films in order to sense and to measure directly adhesion strength *in situ*. As explained before in chapter 3 piezoelectric materials have many advantages as sensors and their

applications in sensing domain are more and more interesting. In the present research advantages as their small thickness, lightness, easy handling and high sensitivity to mechanical load were considered the most.

12 The presented technique is highly sensitive as experimental results were affected by surface roughness.

13 The obtained empirically results demonstrate that ice adhesion strength depends on the surface finish, as it is more finished the adhesion strength is less.

14 The experimental results prove that ice adhesion strength depends significantly on substrate type as the adhesion strength on Plexiglas surface was 100 times less than on the aluminum surface

7.2 Recommendations

Since this work was the one of the first works in this domain in CIGELE laboratory, some recommendations are presented in order to improve and ameliorate test conditions as well as to examine the adhesion strength value under different experimental conditions. Hereafter a list of suggestions is represented for more future works.

1 Investigating the influence of electric field on ice adhesion

Several studies carried out on ice accretion on conductors [1] show that the physical appearance of ice is related to electric field strength and to the polarity of applied voltage. It is likely that atmospheric ice formed under impression of various electric fields exhibit different ice adhesion values. This effect can be a field of interest to investigate.

2 Determining the effects of existing fractures in the interfacial region

Micro-cracks are always present in the interfacial region. The presence of any type of defect at interface would reduce the adhesive strength. Real adhesive joints contain flaws that greatly reduce the practical strength of the adhesive/substrate [19]. Depending on the level of loading, these defects can be the starting point of the creep processes or crack propagation in the interface [36]. In our experimental considerations, the effect of fractures is not taken into account regarding to lack of the necessary experimental equipments. However this aspect seems marginal but it may be interesting in order to attain a better knowledge for producing icephobic materials.

3 Developing a software for automating of amplitude command

In experimental procedure during the test the amplitude of sinusoidal displacement of electromagnetic shaker was increased manually that not ideal for having a good

ramp. It sounds to be great developing particular software in order to control and to increase automatically the amplitude of vibration for desired slope.

4 Studying the ice adhesion on the Phase Change Materials [39]

Briefly Phase Change Materials (PCMs) are 'latent' thermal storage materials. They used chemical bonds to store and release heat. The thermal energy transfer occurs when a material changes from a solid to a liquid or from a liquid to a solid. It would be of great benefit studying the possibility of their application for de-icing purposes; therefore the first thing that seems necessary is researching the ice adhesion strength on them and if the released energy would be adequate for de-icing or not.

5 Trying to measure roughness value empirically for different surface finishes

In order to have the best results and comparisons it is of interest to measure the precise roughness value for different metal surface before tests by means of a profilometer. This gives a clearer image of what happens at the interface.

6 Testing ice adhesion on more different types of materials

It would be of interest carrying out this technique to determine atmospheric ice adhesion strength on various substrates or paintings that are more applicable for instance in aircraft industry, etc.

7 Developing constitutive laws of atmospheric ice

It would be wise if constitutive laws of atmospheric ice are developed to describe theoretically the strain-stress behavior of the atmospheric ice under loading in order to have more knowledge about the physical-mechanical process at interface and to better confront the problem of de-icing.

8 Developing a software to determine automatically the moment of ice de-bonding

Finally, specific software can be developed, using PVDF film signals to automatically detect the precise de-bonding moment and to return the corresponding ice adhesion strength value.

9 Fixing the amplitude of vibration at various level and letting the beam vibrate until failure occurs

The proposed technique involves vibrating a beam which producing an alternating stress at the ice/substrate interface. As shown by experimental studies [37] the loads that do not cause fracture in a single application can result in fracture when applied repeatedly for many cycles (cyclic loading). The phenomenon of fracture under cyclic loading is referred to as Fatigue [29]. This failure apparently results from the fact there are regions usually on the surface or at the interface, where the localized stress is much greater than the average stress acting over the cross section. As this higher stress is cycled, it leads to the initiation of fatigue cracks. Once a fatigue

cracks is initiated, additional cycles of loading cause a further propagation of that crack into the material. Eventually the cross-sectional area of the structure is reduced to some critical size, when the load can no longer be sustained, and as a result sudden fracture occurs [29]. During the cyclic loading fracture of material may occur after a few cycles (low-cycle fatigue) or after millions of cycles (high-cycle fatigue). The number of cycles required to initiate a fatigue crack is called fatigue-initiation life. The period of fatigue-crack growth from initiation to failure is called the fatigue-propagation life. Thus, the total fatigue life is defined as the sum of two lives and it strongly influenced by

- The quality of the surface finish
- The possible residual stress within the member
- The presence of fabrication imperfections such as cracks and defects
- The presence of stress concentrations
- The chemical nature of the environment
- The nature of material itself

It is well-known that the fatigue strength of any material or bond is much less than the static strength and it depends on the number of cycles. The endurance limit is the maximum stress where a bond will not fail after an infinite number of cycles.It may be of great interest studying that using this new technique what strength are measuring One way to test this is to fix the amplitude of vibration at various levels and let the beam vibrate until failure occurs. One can then establish a fatigue curve for the ice/material interface i.e., stress at failure versus number of cycles.

10 Performing the same experiments with de-aired water, distilled, de-ionized and taps water

In this study for all tests the water conductivity was set to its minimum about 5-8 $\mu s / cm$ in order to minimize the probability of affecting charge induced on the piezoelectric film while tap water conductivity is about $80 \mu s / cm$. It may be interesting to perform the same tests with

- De-aired water, which is expected to lead to more adhesion strength;
- Distilled water and de-ionized water in order to eliminate free ions resulted from probable dissolved salts. It can lead to reduce the probability of electrostatic attraction at the interface, thus to reduce the adhesion strength;
- Tap water that is more realistic

11 Carrying out some tests in order to study the influence of ice and substrate thicknesses on stress induced at the interface

As discussed before in chapters 4 and 6 the magnitude of the stress at the aluminium/ice interface is directly linked with the position of the neutral axis (N.A.) and, consequently, it depends directly on the thickness of the ice layer and substrate, as shown in Figure 7.1. Consequently for different ice or substrate thicknesses the magnitude of stress induced at the interface is the not the same. It

can be very interesting to carry out some tests for various thicknesses and comparing two possibilities.

12 Searching a better method for insulating and protecting the PVDF film

In this research in order to avoid a short circuit between the electrodes and the ice layer, a white electrical isolating layer was fixed on the PVDF film before ice accretion, however finding a better technique for PVDF film insulation and protection, in order to have more reliable results, seems necessary

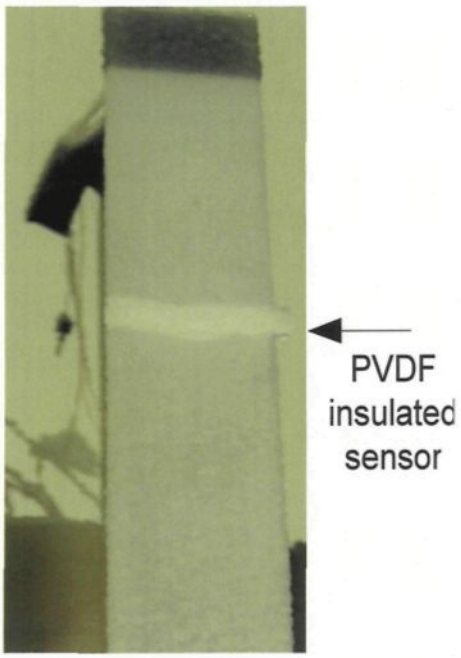

Figure 7.1: Insulating and protecting The PVDF film

13 Considering the effect of temperature

In this study all tests were performed at constant temperature. For future work one can carry out tests at different temperatures in order to study the influence of temperature.

REFERENCES

[1]. Farzaneh, M., "Ice Accretions on High-Voltage Conductors and Insulators and related phenomena", Philosophical Transactions of the Royal Society, Vol. 358, No. 1776, pp. 297-3005, November 2000.

[2]. CEA, « De-Icing Techniques Before, during, and Following Ice Storms », mars 2002.

[3]. http://www.crrel.usace.army.mil/welcome/facilities/Ice_Adhesion_Lab.html

[4]. C. Blakburn, C. Laforte et J.L. Laforte, "Apparatus for Measuring the Adhesion Force of an Thin Ice Sheet on a Substrate", Proceedings of the 9th International Workshop on Atmospheric Icing of Structures, Chester, Royaume-Uni, juin 2000

[5]. Kasaai, M.R.,Farzaneh, M. "A critical evaluation methods of ice adhesion strength on the surface of materials", In Press, Proceedings of OMAE04, 23rd International Conference on Offshore Mechanics and Arctic Engineering, June 20-25, 2004, Vancouver, BC, Canada

[6]. Petrenko, V.F., and Whitworth, R.W., 1999, Physics of Ice, Oxford University Press, Oxford.

[7]. B. Pittenger, D. J. Cook, R. Slaugtherbeck and S. C. Fain, "Investigation of ice-solid interfaces by force microscopy: plastic flow and adhesive forces", J. Vac. Sci. Techno. A16(3), pp. 1832-1837, May/June 1998.

[8]. L. Makkonen, L., and E. Lehmus, ''Studies on adhesion strength of saline ice.'' Proceeding of 9th International Conference on Port and Ocean Engineering Under Arctic Conditions, POAC'87, 1987.

[9]. M. Yoshida, T. Ohichi ,K. Konno, "Adhesion of Ice to Various Materials", Cold Regions Technologies Conference, 29-31 octobre 91, Sapporo, Japon.

[10]. Archer P. Gupta V., "Measurement and control of Ice Adhesion to Aluminium 6061 Alloy", J. Mech. Phys. Solids, Vol. 46, No. 10, pp. 1745-1771, 1998.

[11]. Landy, M., and Freiberger, A. 1967, "Studies of Ice Adhesion, 1:Adhesion of Ice to Plastics", Journal of Colloid and Interface Science, 25,pp.231-244

[12]. www.unisem.com.my/product_reliability8.html

[13]. www.e_materials.Ensiacet.fr/diffusion/diffusion.html

[14]. www.people.ku.edu/~alamgir/cnews.htm

[15]. www.freedrinkingwater.com/water-education/quality-water-filtration-method.htm

[16]. Croutch,V. K., and Hartely, R.A., 1992, "Adhesion of Ice to Coatings and the Performance of Ice release Coatings", journal of Coatings Technology, 64, pp.41-53.

[17]. Hobbs, P.V., 1974, Ice Physics, Clarendon Press,Oxford

[18]. Jellinek, H. H. G., 1962, "Ice Adhesion", Canadian Journal of Physics, 40,pp. 1294-1309

[19]. Gold, L.W., 1970, "Process of Failure in Ice" Canadian Geotechnological Journal, 7, pp. 405-413

[20]. J. M. Sayward, "Seeking low ice adhesion", US Army Regions Research and Engineering Laboratory, New Hamsphire, Special Report AD-A071-040,1979

[21]. Padeletti, G., Pergolin, S., Montesperelli, M., Alessandro, A. D., Campoli, F., and Maltese, P., 2000, "Evaluation of Structural and Adhesive Properties of Nylon 6 and PTFE Alignment Films by Means of Atomic Force Microscopy", Applied Physics, A.71,pp. 571-576

[22]. Krongelb, S., 1978, "Electromagnetic Tensile Adhesion Tests Methods", In Adhesion Measurements of Thin Films, Thick Films and Bulk Coatings, K.L., Mittal, ed., ASTM, Philadelphia , PA, pp. 107-121

[23]. Ahn, J., Mittal, K.L., and McQueen, R.H., 1978, "Hardness and Adhesion of Filmed Structures as Determined by the Scratch Techniques", In: Adhesion Measurement of Thin Films, Thick Films and Bulk Coatings, K.L., mittal, ed., ASTM, Philadelphia, PA., pp. 134-157

[24]. Piezo Film Sensors Technical Manual, electronic Hardware AG, Measurements Specialties, August 1998

[25]. Ueberschlag, "PVDF Piezoelectric Polymer", Sensor Review, Vol. 21, No. 2, April 2001, pp. 118-126

[26]. Loewy, Robert G., "Recent developments in smart structures with aeronautical applications", Review Article, Smart Material structure 6 1997

[27]. L. Ngalamou, N. Noury, E. Chamberod, Ph. Benech "Analysis of sensitivity and the temperature influence of a static force sensor based on a PVDF resonator", Sensors and Actuators A 57 (1996) , pp.173-177

[28]. Yan, Y.J, Yam, L.H. 2003. Mechanical interaction issues in piezoelectric composite structures. Composite Structures. No.59: 61-65.

[29]. Popov E. P. "Engineering mechanics of solids" New Jersey: Prentice Hall, 1998

[30]. S. Timoshenko, Théorie des vibrations, Béranger, 1945

[31]. Y. Jullien, Vibration des systèmes continues, GALF, 1971

[32]. D. V. Bambill, S. J. Escanes, C.A. Rossit, "Forced vibration of a clamped free beam with a mass at the free end with an external periodic disturbance acting on the mass with application in ships' structures" Ocean Engineering, vol. 30, pp. 1065-1077, 2003

[33]. D.J. Inman Engineering vibration New Jersey: Prentice Hall,1994

[34]. Braun, S.; Ewins, D.;Rao, S.S., "Encyclopedia of Vibration" San Diego: Academic Press,V.1, pp.137, 2002

[35]. L. Ngalamou, N. Noury, E. Chamberod, Ph. Benech "Analysis of sensitivity and the temperature influence of a static force sensor based on a PVDF resonator", Sensors and Actuators A, vol.57, pp.173-177, 1996

[36]. Raraty, L.W., and Tabor, D., 1958, "The Adhesion and Strength Properties of Ice" Proceeding of Royal society of London, series A, Mathematical and Physical Sciences, London, Vol. 245, pp. 184-201

[37]. Collins, J.A, "Failures of Materials in Mechanical Design" New York, John Wiley &Sons,1981

[38]. http://hyperphysics.phy-astr.gsu.edu/hbase/kinetic/relhum.html

[39]. Anderson, J.C., Leaver, K.D., Leavers P., Rawlings, R.D., " Material Science for Engineering" 5th edition, CRC Press, 2003

APPENDIX

Appendix[19]

A. Stress

A.1 Normal Stress

If the internal sectioned area is subdivided into smaller and smaller areas, ΔA, two important assumptions must be made regarding to the material: it is continuous and it is cohesive. Thus, as the subdivided area is reduced to infinitesimal size, the distribution of internal forces acting over the entire sectioned area will consist of an infinite number of forces each acting on an element, ΔA, as a very small force ΔF. The ratio of incremental force to incremental area on which the force acts such that: $\lim_{\Delta A \to 0} \frac{\Delta F}{\Delta A}$ is the stress that can be further defined as the intensity of the internal force on a specific plane (area), passing through a point.

Stress has two components, one acting perpendicular to the plane of the area and the other acting parallel to the area. Mathematically, the former component is expressed as a normal stress that is the intensity of the internal force acting normal to an incremental area such that,

[19] This Appendix is derived from [29]

$$\sigma = \lim_{\Delta A \to 0} \frac{\Delta F_n}{\Delta A} \qquad \text{Eq.A.1}$$

Where $+\sigma$ is tensile stress, i.e., "pulling" stress, and $-\sigma$ is compressive stress, i.e., "pushing" stress.

A.2 Shear Stress

The other stress component is expressed as shear stress, which is the intensity of the internal force acting tangent to an incremental area such that:

$$\tau = \lim_{\Delta A \to 0} \frac{\Delta F_t}{\Delta A} \qquad \text{Eq.A.2}$$

The general state of stress is one that includes all the internal stresses acting on an incremental element. In particular, the most general state of stress must include normal stresses in each of the three Cartesian axes, and six corresponding shear stresses.

Note that for the general state of stress that $+\sigma$ acts normal to a positive face in the positive coordinate direction and an $+\tau$ acts tangent to a positive face in a positive coordinate direction. For example, σ_{xx} (or just σ_x) acts normal to the positive x face in the positive x direction and τ_{xy} acts tangent to the positive x face in the positive y-direction.

Although in the general stress state, there are three normal stress component and six shear stress components, by summing forces and summing moments it can be shown that $\tau_{xy} = \tau_{xy}; \tau_{xz} = \tau_{zx}; \tau_{zy} = \tau_{yz}$, which is out of the scope of this study.

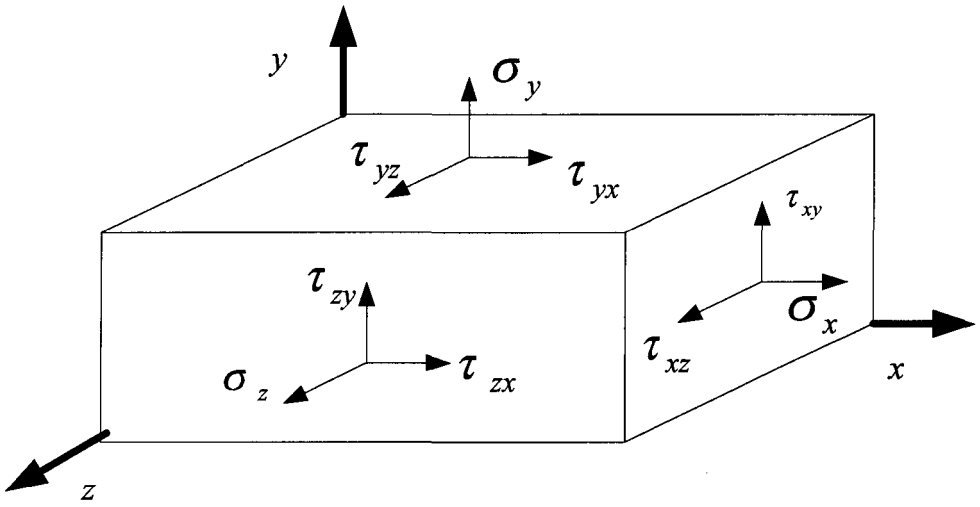

Figure A.1: Demonstration of three normal stresses and six shear stresses

Therefore the complete state of stress contains six independent stress components (three normal stresses σ_x in x-direction, σ_y in y-direction and σ_z in z-direction as well as three shear stresses $\tau_{xy}; \tau_{yz}$ and τ_{zx}) which uniquely describe the stress state for each particular orientation. This complete state of stress can be written in vector form as following,

$$\begin{bmatrix} \sigma_x & \sigma_y & \sigma_z & \tau_{xy} & \tau_{yz} & \tau_{zx} \end{bmatrix}^T \qquad \text{Eq.A.3}$$

Otherwise, in matrix form it can be written as

$$\begin{bmatrix} \sigma_x & \tau_{xy} & \tau_{xz} \\ \tau_{xy} & \sigma_y & \tau_{yz} \\ \tau_{xz} & \tau_{yz} & \sigma_z \end{bmatrix} \qquad \text{Eq.A.4}$$

A particular set of coordinates exist that diagnolize the stress tensor as following

$$\begin{bmatrix} \sigma_1 & 0 & 0 \\ 0 & \sigma_2 & 0 \\ 0 & 0 & \sigma_3 \end{bmatrix} \qquad \text{Eq.A.5}$$

The stress vector depends on the location of the point as well as the orientation of the surface through the point. This figure shows all of the stress forces that act on the infinitesimal element (more details about these forces in Equilibrium equations section).

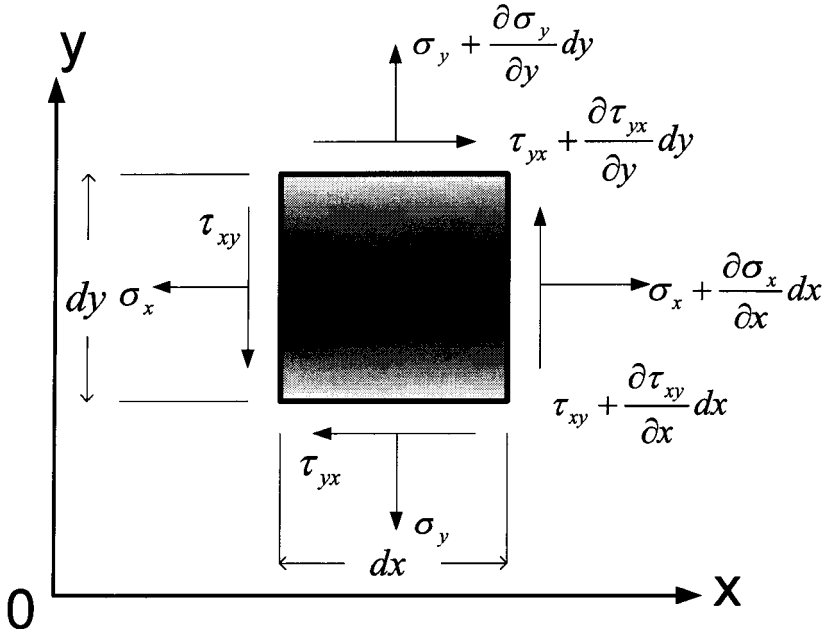

Figure A.2: All of the stress forces act on the infinitesimal element

The unit of stress in SI is,

$$\frac{force}{area} = \frac{F}{L^2} = \frac{N}{m^2}$$

Often it is necessary to find the stresses in a particular direction rather than just calculating them from the geometry of simple parts. For the one-dimensional case shown in Figure A.3 the applied force, P, can be written in terms of its normal, P_N and tangential, P_T, components which are functions of the angle, θ, such that:

$$P_T = P\sin\theta \qquad \text{Eq.A.6}$$

$$P_N = P\cos\theta \qquad \text{Eq.A.7}$$

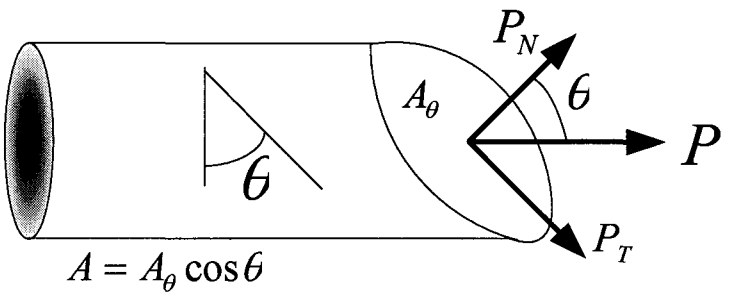

Figure A.3: Calculating the stress in a particular direction

The area A_θ, on which P_N and P_T act can also be written in terms of the area, A, normal to the applied load P, and the angle θ,

$$A_\theta = A/\cos\theta \qquad \text{Eq.A.8}$$

The normal and shear stress relation acting on any area oriented at angle, θ relative to the original applied force, P are:

$$\sigma_\theta = \frac{P_N}{A_\theta} = \frac{P\cos\theta}{A/\cos\theta} = \frac{P}{A}\cos^2\theta = \sigma\cos^2\theta \qquad \text{Eq.A.9}$$

$$\tau_\theta = \frac{P_T}{A_\theta} = \frac{P\sin\theta}{A/\cos\theta} = \frac{P}{A}\cos\theta\sin\theta = \sigma\cos\theta\sin\theta \qquad \text{Eq.A.10}$$

where σ is the applied unidirectional normal stress.

B. Strain

Whenever a force is applied to a body, it will tend to change the body's shape and size. There changes are referred to as deformation. Size changes are known as dilatation (volumetric changes) and are due to normal stresses. Shape changes are known as distortion and are due to shear stresses. In order to describe the deformation in length of line segments and the changes in angles between them, the concept of strain is used. Therefore, strain is defined as normalized deformations within a body exclusive of rigid body displacements.

These are two types of strain, one producing size changes by elongation or contraction named as normal strain and the other producing shape changes by angular distortion named as shear strain.

B.1 Normal Strain

Normal strain is the elongation or contraction of a line segment per unit length resulting in a volume change such that:

$$\varepsilon = \lim_{B \to A} \frac{A'B' - AB}{AB} = \frac{L_f - L_0}{L_0} \qquad \text{Eq.A.11}$$

where all the parameters are determined by Figure A.4,

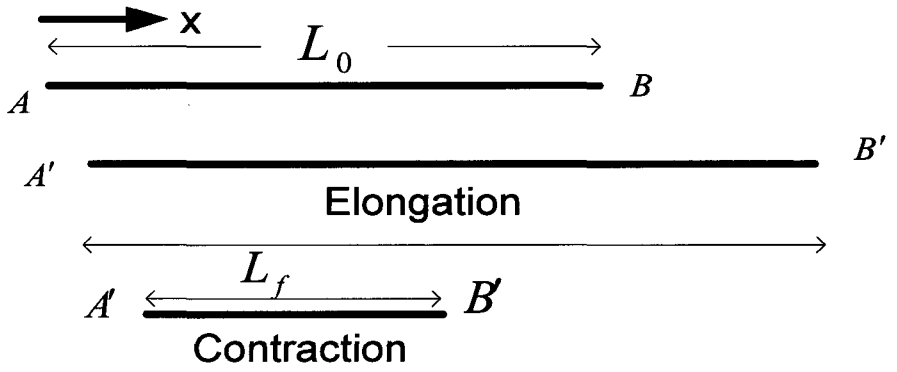

Figure A.4: Simple illustration of normal strain forms as elongation and contraction

where $+\varepsilon$ is tensile strain or elongation and $-\varepsilon$ is compressive strain or contraction.

B.2 Shear Strain

Shear strain is the angle change between two line segments resulting in a shape change as shown in Figure A.5, thus

$$\gamma = \left(\theta = \frac{\pi}{2}\right) - \theta' \approx \frac{\Delta}{h} \qquad \text{(For small angles)} \qquad \text{Eq.A.12}$$

where $+\gamma$ occurs if $\frac{\pi}{2} > \theta'$ and $-\gamma$ occurs if $\frac{\pi}{2} < \theta'$

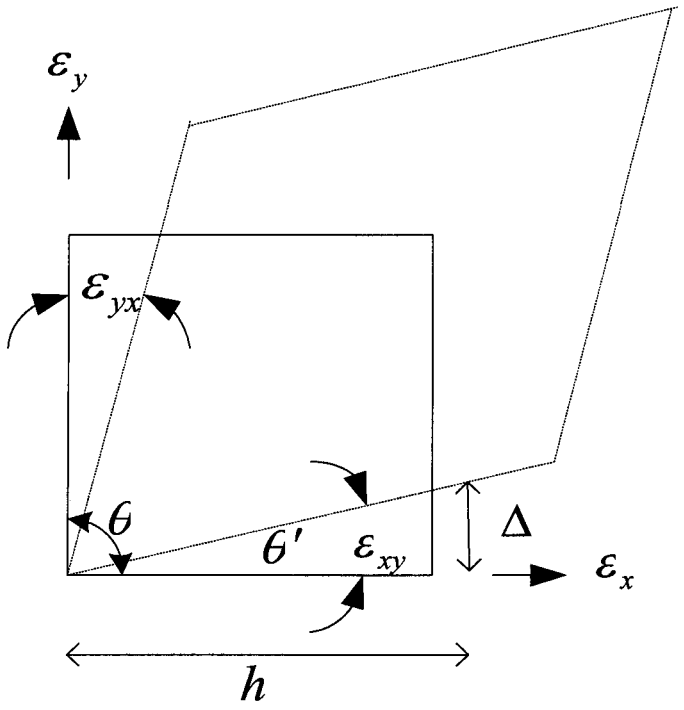

Figure A.5: Engineering shear strain, $\gamma_{xy} = \varepsilon_{xy} + \varepsilon_{yx}$

The complete state of strain has six independent strain components (three normal strains $\varepsilon_x, \varepsilon_y$ and ε_z as well as three engineering shear strains, $\gamma_{xy}; \gamma_{yz}; \gamma_{xz}$) which uniquely describe the strain state for each particular orientation. This complete state of strain can be written in vector form as,

$$\begin{bmatrix} \varepsilon_x & \varepsilon_y & \varepsilon_z & \gamma_{xy} & \gamma_{xz} & \gamma_{yz} \end{bmatrix}^T \qquad \text{Eq.A.13}$$

Alternatively, the complete state of strain can be written in matrix form as,

$$\begin{bmatrix} \varepsilon_x & \gamma_{xy} & \gamma_{xz} \\ \gamma_{xy} & \varepsilon_y & \gamma_{yz} \\ \gamma_{xz} & \gamma_{yz} & \varepsilon_z \end{bmatrix} \qquad \text{Eq.A.14}$$

The unit of strain in SI is $\frac{length}{length} = \frac{L}{L} = \frac{m}{m}$

C. Strain-Displacement Relation

A displacement field describes how a body deforms as well as how it displaces. Strain-displacement relations extract the strain field contained in a displacement field. The definition of strain is considered to obtain this field,

- Normal strain is change in length divided by original length, Shear strain is the amount of change in a right angle.
- X-direction displacement u as well as Y-direction displacement v are functions of coordinates; $u = u(x, y, z)$ and $v = v(x, y, z)$.

Therefore two-dimensional strain-displacement relations are as,

$$\varepsilon_x = \frac{\partial u}{\partial x}; \varepsilon_x = \frac{\partial v}{\partial y}; \gamma_{xy} = \frac{\partial u}{\partial y} + \frac{\partial v}{\partial x} \qquad \text{Eq.A.15}$$

In matrix operator format, the strain-displacement relations are:

$$\begin{Bmatrix} \varepsilon_x \\ \varepsilon_y \\ \gamma_{xy} \end{Bmatrix} = \begin{bmatrix} \frac{\partial}{\partial x} & 0 \\ 0 & \frac{\partial}{\partial y} \\ \frac{\partial}{\partial y} & \frac{\partial}{\partial x} \end{bmatrix} \begin{Bmatrix} u \\ v \end{Bmatrix} \Rightarrow \{\varepsilon\} = [\partial]\{u\} \qquad \text{Eq.A.16}$$

D. Stress - Strain Relationships (Constitutive Relations)

If deformation and strain are the response of the body to an applied force or stress, then there must be some type of relations, which allow the strain to be predicted from stress. This relation is called constitutive model of a material and conveys the most important mechanical properties of a material during a loading process. The constitutive model of a material is based on results from experiments performed under very simple loading conditions. When a constitutive relation is combined with the equilibrium and compatibility equations, general structural behavior can be predicted.

During uni-axial loading by load, P, of a rod with uniform cross sectional area, A, and length, L, the applied stress, σ is simply calculated as,

$$\sigma = \frac{P}{A}$$ Eq.A.17

The resulting normal strain, ε_l in the longitudinal direction can be calculated from the deformation response, Δl along the L direction:

$$\varepsilon_L = \frac{\Delta L}{L}$$ Eq.A.18

The normal strain, ε_r in the transverse direction can be calculated from the deformation response, ΔD along the D direction:

$$\varepsilon_T = \frac{\Delta D}{D}$$ Eq.A.19

There is a constant of proportionality between stress and strain in the elastic region such that

$$y = mx + b \Rightarrow \sigma = E\varepsilon$$ Eq.A.20

where $E = \frac{\Delta\sigma}{\Delta\varepsilon}$ is known as the elastic modulus or Young's modulus and above equation is known as unidirectional Hook's law.

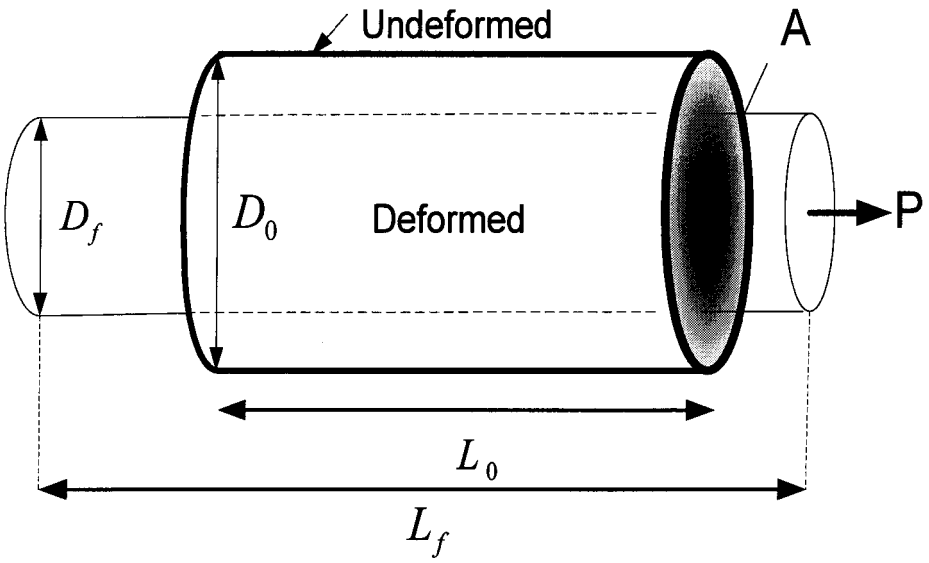

Figure A.6: Uni-axially loaded rod undergoing longitudinal and transverse deformation

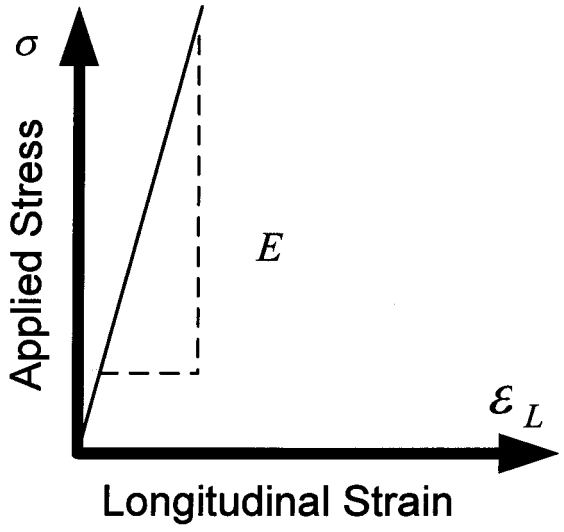

Figure A.7: Stress versus longitudinal strain

A plot of ε_T vs. ε_L shows a constant of proportionality between transverse and longitudinal strains in the elastic region such that

$$y = mx + b \Rightarrow \varepsilon_T = -\nu\varepsilon_L \qquad \text{Eq.A.21}$$

where $\nu = -\frac{\varepsilon_r}{\varepsilon_l}$ is known as Poisson's ratio (which will be explained after).

For the results for three different uni-axial stresses applied separately, x, y and z can give the general relations between normal stress and normal strain known as generalized Hook's law if the strain components for each of the stress conditions are superposed:

$$\varepsilon_x = \frac{1}{E}\left(\sigma_x - \nu\left(\sigma_y + \sigma_z\right)\right) \qquad \text{Eq.A.22}$$

$$\varepsilon_y = \frac{1}{E}\left(\sigma_y - \nu\left(\sigma_x + \sigma_z\right)\right)$$

$$\varepsilon_z = \frac{1}{E}\left(\sigma_z - \nu\left(\sigma_x + \sigma_y\right)\right)$$

Since shear stresses are decoupled (i.e., unaffected) by stresses in other directions the relations for shear stress-shear strain are:

$$\gamma_{xy} = \frac{1}{G}\tau_{xy}$$

Eq.A.23

$$\gamma_{xz} = \frac{1}{G}\tau_{xz}$$

$$\gamma_{yz} = \frac{1}{G}\tau_{yz}$$

where the shear modulus is $G = \frac{\Delta\tau}{\Delta\gamma} = \frac{E}{2(1+\nu)}$.

Generalized Hook's law is usually written in matrix form such that:

$$\begin{Bmatrix} \varepsilon_x \\ \varepsilon_y \\ \varepsilon_z \\ \gamma_{xy} \\ \gamma_{xz} \\ \gamma_{yz} \end{Bmatrix} = \begin{bmatrix} \frac{1}{E} & \frac{-\nu}{E} & \frac{-\nu}{E} & 0 & 0 & 0 \\ \frac{-\nu}{E} & \frac{1}{E} & \frac{-\nu}{E} & 0 & 0 & 0 \\ \frac{-\nu}{E} & \frac{-\nu}{E} & \frac{1}{E} & 0 & 0 & 0 \\ 0 & 0 & 0 & \frac{1}{G} & 0 & 0 \\ 0 & 0 & 0 & 0 & \frac{1}{G} & 0 \\ 0 & 0 & 0 & 0 & 0 & \frac{1}{G} \end{bmatrix} \begin{Bmatrix} \sigma_x \\ \sigma_y \\ \sigma_z \\ \tau_{xy} \\ \tau_{xz} \\ \tau_{yz} \end{Bmatrix}$$

Eq.A.24

Therefore,

$$\begin{Bmatrix} \sigma_x \\ \sigma_y \\ \sigma_z \\ \tau_{xy} \\ \tau_{xz} \\ \tau_{yz} \end{Bmatrix} = \begin{bmatrix} \frac{E}{1+\nu}\left[1+\frac{\nu}{1-2\nu}\right] & \frac{\nu E}{(1+\nu)(1-2\nu)} & \frac{\nu E}{(1+\nu)(1-2\nu)} & 0 & 0 & 0 \\ \frac{\nu E}{(1+\nu)(1-2\nu)} & \frac{E}{1+\nu}\left[1+\frac{\nu}{1-2\nu}\right] & \frac{\nu E}{(1+\nu)(1-2\nu)} & 0 & 0 & 0 \\ \frac{\nu E}{(1+\nu)(1-2\nu)} & \frac{\nu E}{(1+\nu)(1-2\nu)} & \frac{E}{1+\nu}\left[1+\frac{\nu}{1-2\nu}\right] & 0 & 0 & 0 \\ 0 & 0 & 0 & G & 0 & 0 \\ 0 & 0 & 0 & 0 & G & 0 \\ 0 & 0 & 0 & 0 & 0 & G \end{bmatrix} \begin{Bmatrix} \varepsilon_x \\ \varepsilon_y \\ \varepsilon_z \\ \gamma_{xy} \\ \gamma_{xz} \\ \gamma_{yz} \end{Bmatrix}$$

Eq.A.25

Generalized Hook's law can be simplified somewhat for the special case of plane stress in the x-y plane since σ_z=0. Being orthogonal to the x-y plane, since σ_z is an also a principal stress by definition, all the shear stresses associated with the z-direction are also zero. Thus, the stress-strain relations for plane stress in the x-y plane become,

$$\begin{Bmatrix}\sigma_x\\ \sigma_y\\ \tau_{xy}\end{Bmatrix}=\begin{bmatrix}\frac{E}{(1-\nu^2)} & \frac{\nu E}{(1-\nu^2)} & 0\\ \frac{\nu E}{(1-\nu^2)} & \frac{E}{(1-\nu^2)} & 0\\ 0 & 0 & G\end{bmatrix}\begin{Bmatrix}\varepsilon_x\\ \varepsilon_y\\ \gamma_{xy}\end{Bmatrix}\Rightarrow\{\sigma\}=[E]\{\varepsilon\} \qquad \text{Eq.A.26}$$

For the special case of plane stress, although σ_z =0, the strain in the z-direction is not zero but instead can be determined such that

Plane stress: $\sigma_z=0,\quad \varepsilon_z\neq 0=-\frac{\nu}{1-\nu}(\varepsilon_x+\varepsilon_y)$

Similarly for the special case of plane strain, although, $\varepsilon_z=0$, the stress in the z-direction is not zero but instead can be determined such that

Plane strain: $\varepsilon_z=0,\ \sigma_z\neq 0=\nu(\sigma_x+\sigma_y)$

Experiments, mainly tension or compression tests, provide basic information on the mechanical behavior of materials under load. In these experiments, the macroscopic (overall) response of specimens to the applied load is observed in order to determine force-deformation relationships.

E. Poisson Ratio

In addition to the deformation of materials in the direction of applied force , another property can be observed in all solid materials __ namely, that at right angles to the applied uni-axial force, a certain amount of lateral (transverse) expansion or contraction takes place. If a solid body is subjected to an axial tension, it contracts laterally; on the other hand, if it is compressed, the material "squashes out" sideways. For a general theory, it is preferable to refer to those lateral deformations based on deformation per unit of length of the transverse dimension. These relative unit lateral deformations are termed lateral strains. Moreover, it is known from experiments that lateral strain bear a constant relationship to the longitudinal or axial strains caused by axial force, provided a material remains elastic, homogenous, and isotropic. This property is called Poisson's Ratio and it is defined as follows:

$$\nu = \left| \frac{lateral\_strain}{axial\_strain} \right| = -\frac{lateral\_strain}{axial\_strain} \qquad \text{Eq.A.27}$$

The value of ν fluctuates for different materials over a relatively narrow range. Generally, it is in order of 0.25 to 0.35.

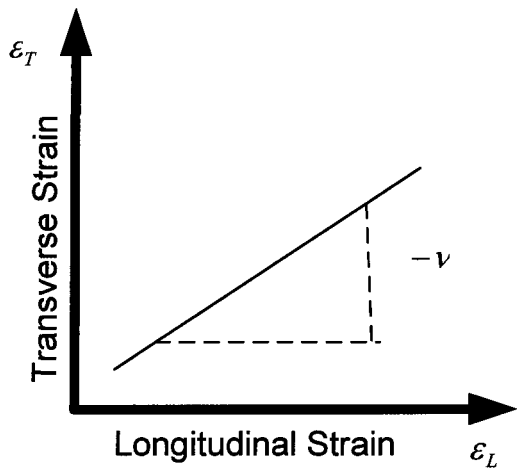

Figure A.8: Transverse strain versus longitudinal strain

F. Engineering Stress-Strain Diagrams

In the experimental study of the mechanical properties of materials, it is customary to plot diagrams of the relationship between stress and strain in a particular test. The stress-strain diagrams are independent of the size of the specimen. The general shape of stress-strain diagram for a ductile steel specimen loaded in tension or failure for a monotonically increasing load is shown in the following figure (the normal stress versus engineering strain). This figure can be subdivided into four well-defined regions:

1. the linear elastic region
2. the yield plateau
3. the strain-hardening region
4. the post ultimate stress or strain-softening region

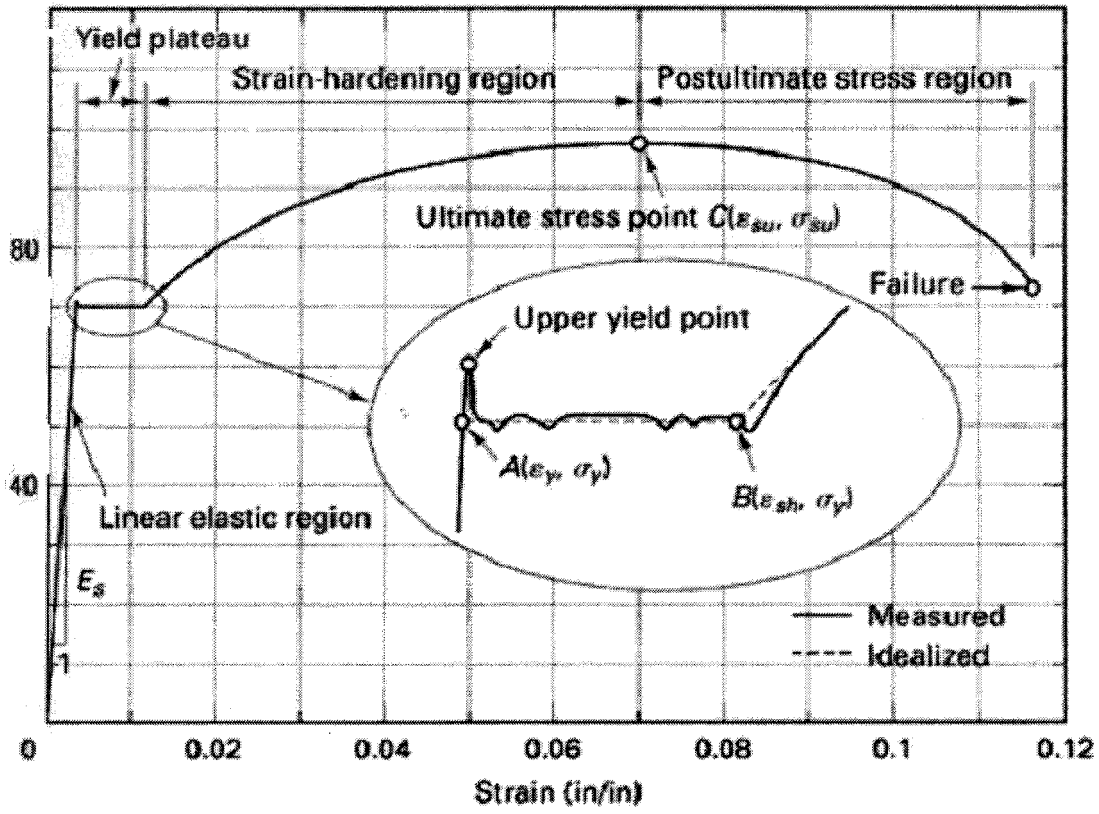

Figure A.9: Engineering Stress-strain diagrams [29]

This diagram is very important in engineering since it provides the means for obtaining various mechanical properties of a material without regard to its physical size or shape. In some engineering applications, the strain may be large. For such purposes the total strain will be defined as a sum of incremental strains; thus

$$\bar{\varepsilon} = \sum \Delta\bar{\varepsilon} = \sum \frac{\Delta L}{L} \qquad \text{Eq.A.28}$$

where L is the current gage length when the increment of elongation or contraction ΔL occurs. If L_0 is the initial gage of the specimen, then in the limit as $\Delta L \to 0$ strain corresponding to the gage length L_f can be defined by the following integral:

$$\bar{\varepsilon} = \int_{L_0}^{L_f} \frac{dL}{L} = \ln\left(\frac{L_f}{L_0}\right) \qquad \text{Eq.A.29}$$

This strain, obtained by adding up the increments of strains, is called logarithmic strain or true strain During plastic strain of a uniform specimen subjected to axial tension (compression), the cross-section area gets smaller (larger) as the specimen elongates (shortens). A more accurate description of the actual stress experienced by the specimen can be given by the true stress concept. The true stress is related to instantaneous cross-sectional area and the applied force as

$$\bar{\sigma} = \frac{F}{A} \qquad \text{Eq.A.30}$$

Since plastic strain involves no volume change, that is, $A_0 L_0 = AL$ and $L = L_0(1+\varepsilon)$

$$\overline{\sigma} = \frac{F}{A_0}(1+\varepsilon) = \sigma(1+\varepsilon)$$

Eq.A.31